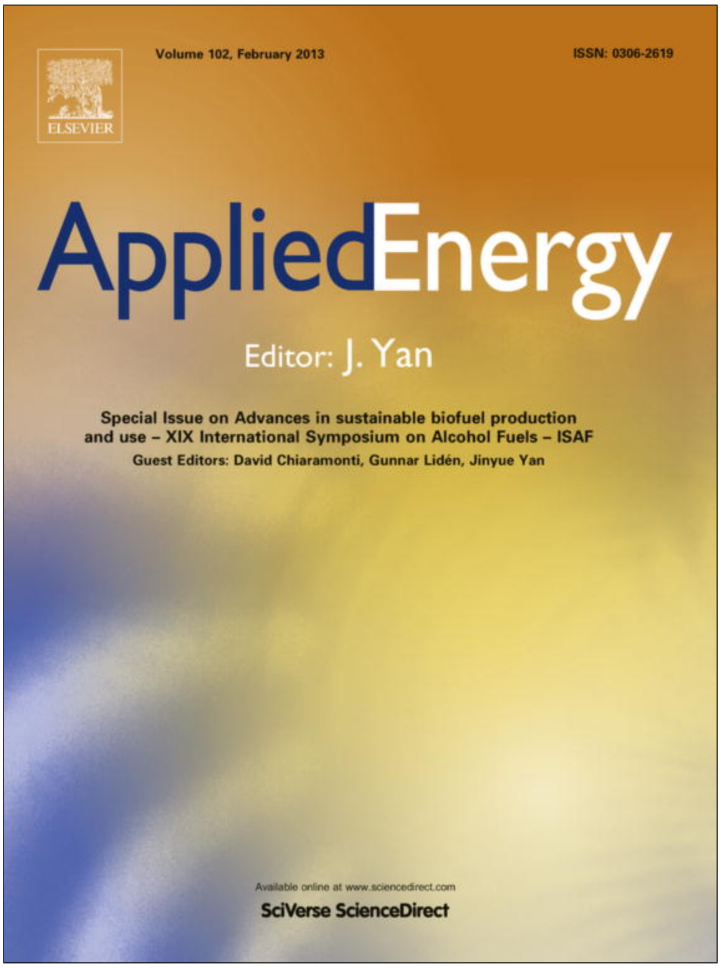
Volume 102, February 2013
ISSN: 0306-2619
ELSEVIER
AppliedEnergy
Editor: J. Yan
Special Issue on Advances in sustainable biofuel production and use – XIX International Symposium on Alcohol Fuels – ISAF
Guest Editors: David Chiaramonti, Gunnar Lidén, Jinyue Yan
Available online at www.sciencedirect.com
SciVerse ScienceDirect

Applied Energy 102 (2013) 1160–1177

Contents lists available at SciVerse ScienceDirect

Applied Energy

journal homepage: www.elsevier.com/locate/apenergy

A procedure to calculate the five-parameter model of crystalline silicon photovoltaic modules on the basis of the tabular performance data

Aldo Orioli *, Alessandra Di Gangi

D.d.E. Dipartimento dell'Energia, Università degli Studi di Palermo, Viale delle Scienze Edificio 9, 90128 Palermo, Italy

HIGHLIGHTS

- ▶ Accurate predictive tools for PV systems require a wide set of graphical performance data.
- ▶ We set up a procedure to evaluate the one-diode equivalent circuit using tabular performance data.
- ▶ Correlations based on the survey of more than 100 PV module characteristics were defined.
- ▶ We tested the new model comparing the results with the data measured by different manufacturers.

ARTICLE INFO

Article history:
Received 6 February 2012
Received in revised form 8 May 2012
Accepted 14 June 2012
Available online 21 July 2012

Keywords:
Photovoltaic modules
Five-parameter model
I–V characteristics
Solar energy

ABSTRACT

Only few manufactures provide the wide set of graphical data that are necessary to use high performance predictive tools for PV systems. On the other hand, reliable graphical data require accurate laboratory measurements that increase manufacturing costs. For this reason PV system designers have to choose between the use of cheap PV modules, lacking in technical data, and the reliable energy predictions that are possible only if the current–voltage characteristics are provided by the PV module manufacturers.

This paper describes the procedure to evaluate the parameters of a one-diode equivalent circuit able to accurately represent the electrical behaviour of a PV panel by means of the minimum set of technical data that are usually provided by all manufacturers. To reach the purpose some correlations based on the survey of more than one hundred PV module characteristics were defined to make up for the lack of technical information. The computer routines used to evaluate the values of the model parameters are listed; the routines are written in BASIC and can be easily implemented, even like VBA macros in Microsoft Excel.

The capability of the new model to calculate the current–voltage characteristics was tested by comparing the results with data measured by four different manufacturers. The results of the application of the new model confirm the reliability of the proposed procedure. The differences between the calculated and the measured data are always less than the data tolerance usually declared by the manufacturers.

1. Introduction

The accurate modelling of photovoltaic (PV) modules is of primary concern because it allows the designer to optimize the system performance and to maximize the cost effectiveness of the system. The performance of a PV system depends on many important features such as the site latitude, the tilt and azimuth angles of the panel and the shadowing obstructions; these features mainly affect the amount of solar energy collected by the panels that can be converted into electricity. Although the knowledge of the available solar energy is the first step to estimate the performance of a PV system, it is the conversion efficiency of the panels that plays a main role as it quantifies the electric power produced. The conversion efficiency mainly depends on solar irradiation, silicon slab operating temperature and electrical load; the influence of these physical parameters, which are usually very variable during the time, must be carefully taken into account when reliable predictions of a PV system performances are required.

Estimates based on constant values of the conversion efficiency, or on values derived from a simplistic description of the physical phenomena, will yield erroneously optimistic economical predictions. Cautious predictions are needed because other features can be unforeseeable or difficult to assess. The decline in performance due to long-term sun and weather exposure, or the need for device substitution can definitely affect system effectiveness during real operation. Although the rapid decrease in the PV module cost and the escalation in the price of petrochemical fuels have encouraged the diffusion of PV systems, their payback period is

* Corresponding author. Tel.: +39 09123861905; fax: +39 091484425.
E-mail addresses: aldo.orioli@unipa.it, orioli@dream.unipa.it (A. Orioli).

0306-2619/$ - see front matter © 2012 Elsevier Ltd. All rights reserved.
http://dx.doi.org/10.1016/j.apenergy.2012.06.036

Nomenclature

G	solar irradiance (W/m^2)
G_{NOCT}	irradiance used in defining T_{NOCT} (800 W/m^2)
G_{ref}	solar irradiance at SRC (1000 W/m^2)
I	current generated by the panel (A)
I_L	photocurrent (A)
I_L^*	photocurrent at $T = T^*$ (A)
I_{mp}	current at the maximum power point (A)
I_{sc}	short circuit current of the panel (A)
I^*	current generated by the panel at $T = T^*$ (A)
I_{max}^*	current generated by the panel at $T = T^*$ and $P^* = P_{max}^*$ (A)
I_0	reverse saturation current (A)
I_0^*	reverse saturation current at $T = T^*$ (A)
k	Boltzmann constant (J/K)
K	thermal correction factor (Ω/°C)
n	diode quality factor
N_{cs}	number of cells connected in series
P^*	power generated by the PV panel at $T = T^*$ (W)
P_{max}	maximum power generated by the PV panel at SRC (W)
P_{max}^*	maximum power generated by the PV panel at $T = T^*$ (W)
q	electron charge (C)
R_L	electrical load (Ω)
R_s	series resistance (Ω)
R_{so}	reciprocal of slope of the I–V characteristic of the PV panel for $V = V_{oc}$ and $I = 0$ (Ω)
R_{sh}	shunt resistance (Ω)
R_{sho}	reciprocal of the slope of the I–V characteristic of the PVpanel for $V = 0$ and $I = I_{sc}$ (Ω)
q	electron charge (C)
T	temperature of the PV cell (°K)
T_a	ambient temperature (°C)
T_{NOCT}	nominal operating cell temperature (°C)
T_{ref}	temperature of the PV panel at SRC (25 °C – 298.15°K)
$T*$	temperature of the PV panel different from T_{ref} (°K)
V	voltage generated by the PV panel (V)
V_d	voltage across the diode (V)
$V_{d,max}$	voltage across the diode at the maximum power (V)
V_{mp}	voltage at the maximum power point (V)
V_{oc}	open circuit voltage of the PV panel (V)
$V_{oc,ref}$	open circuit voltage of the PV panel at SRC (V)
V^*	voltage generated by the PV panel at $T = T^*$ (V)
V_{max}^*	voltage generated by the panel at $T = T^*$ and $P^* = P_{max}^*(V)$
α_G	ratio between the current irradiance and the irradiance at SRC
β	temperature coefficient (K^{-1})
γ	ideality factor
δ	solar radiation coefficient
η	efficiency of the PV panel
η_{ref}	efficiency of the PV panel at SRC
$\mu_{I,sc}$	thermal coefficient of the short circuit current (A/°C)
$\mu_{P,max}$	thermal coefficient of the maximum power (%/°C)
$\mu_{V,oc}$	thermal coefficient of the open circuit voltage (V/°C)

still quite long because the value of the efficiency of the panels is less than 20%.

In order to accurately assess the performance of a PV system, very reliable and effective predictive tools are necessary. Generally speaking, the reliability of the information derived by a predictive tool is related to the quality of the description of the physical phenomena and to the amount of input data used to perform the calculations. A good predictive tool should be sensitive to all physical parameters that can influence the results of predictions. Predicted results agree with the actual performance of the system during operation only if the phenomena are adequately described by the used equations. Moreover the input data set must contain the peculiar physical characteristics of the analysed devices. Obviously, the data related to the characteristics of the devices should be the result of accurate laboratory measurements performed on the PV panels.

Predictive performance tools are widely used by engineers to design plants composed of components with characteristics and performance data that are issued by manufacturers. The majority of the hundreds of global PV panel manufacturers issue datasheets that can be downloaded online from the Internet. Unfortunately the information provided by the PV module manufactures rarely allows one to thoroughly exploit high-performance predictive tools. An analysis of information from more than 400 manufacturer websites was carried out; unfortunately it affirms that the quality of this information is variable and, sometimes, is almost useless for producing a reliable design. Frequently, only a few tabular data concerning the maximum power voltage and current, the short circuit current, and the open circuit voltage are provided. A small percentage of manufacturers provide the current–voltage (I–V) characteristics of the panel; the graphical data provided are often unusable because they are incoherent and discordant.

When the available technical data are insufficient or unreliable it is vain to use high performance PV panel predictive tools because the procedures used to calculate the parameters of the equivalent circuit may abort for lack of information. It would be better to use an even less accurate predictive tool that is able to adequately represent the electrical behaviour of a PV panel by means of the minimum set of technical data that are usually provided by all manufacturers.

2. Photovoltaic panel models

Different approaches to get reliable predictive tools for PV panels have been adopted. Some authors studied analytical correlations [1,2], and others used equivalent electrical circuits that assimilate a PV cell to an illuminated semiconductor diode whose current–voltage characteristic was described by Shockley [3] with the equation:

$$I = I_L - I_0\left(e^{\frac{qV}{\gamma kT}} - 1\right) \tag{1}$$

where I_L is the photocurrent generated by illumination, I_0 is the reverse saturation current of the diode, q is the electron charge (1.602×10^{-19} C), k is the Boltzmann constant (1.381×10^{-23} J/K), T is the junction temperature and γ that, in compliance with the traditional theory of semiconductors [4], is 1 for germanium and approximately 2 for silicon. According to Eq. (1), a PV cell can be represented by a current source with intensity I_L, connected in parallel with a diode. As Wolf [5] observed, in a PV cell, the photocurrent is not generated by only one diode but is the global effect of the presence of a multitude of flanked diodes that are uniformly distributed throughout the surface that separates the two semiconductor slabs. For this reason Wolf described the PV cell with an equivalent electric circuit containing a multitude of different lumped elementary components, each one made up of a current generator, a diode and a series resistance. Such an equivalent circuit was too complex to be used, and a simplified equivalent circuit was eventually proposed. The circuit contains only one pair of diodes, a current generator and two resistors, R_s and R_{sh}, which are employed

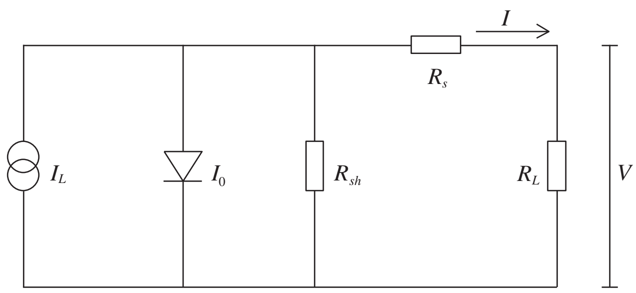

Fig. 1. One-diode equivalent circuit for a PV panel.

to take into account of dissipative effects and construction defects that can cause parasite currents within the PV cell.

The two-diode model requires the determination of seven parameters that variously affect the shape of the *I–V* characteristic. The solution of the seven-parameter equivalent circuit, which is not easy because of the implicit form of the equation and the presence of two exponential terms, was faced assuming some analytical simplifications [6–9] or by means of optimization and evolutionary algorithms [10,11]. The cited methods are very sensitive to the initial conditions and, if not properly guided by an initial estimate of the parameters, may lead to inconsistent results. For this reason some authors preferred to use a simplified model with a single diode (Fig. 1),

which is described by the following five-parameter equation:

$$I = I_L - I_0\left(e^{\frac{V+IR_s}{nT}} - 1\right) - \frac{V + IR_s}{R_{sh}} \quad (2)$$

where following traditional theory, the photocurrent I_L depends on solar irradiance, the reverse saturation current I_0 is affected by silicon temperature and n, R_s and R_{sh} are constant. Coefficient n contains q, k, γ and the number of cells of the panel that are connected in series. Despite its simplicity, the one-diode model adequately fits with the *I–V* characteristic at standard rating conditions (SRC) – irradiance G_{ref} = 1000 W/m^2, cell temperature T_{ref} = 25 °C and average solar spectrum at AM 1.5 – of most of the modern and efficient PV modules that, since they have a small R_s and a great R_{sh}, show a good fill factor and, consequently, a *I–V* characteristic with a very sharp bent. Many authors have focused on the one-diode model and have recently proposed some interesting improvements that allow the determination of the five parameters on the basis of the performance data typically provided by manufactures [12–18]. The proposed procedures require the following input data set:

- open circuit voltage V_{oc} and short circuit current I_{sc} at SRC;
- voltage V_{mp} and current I_{mp} at the maximum power at SRC;
- reciprocal R_{so} and R_{sho} of the slope of the *I–V* characteristic in the open circuit point and in the short circuit point at SRC, respectively;
- open circuit voltage temperature coefficient $\mu_{V,oc}$ and short circuit current temperature coefficient $\mu_{I,sc}$.

The information available in the datasheets usually concerns V_{oc}, I_{sc}, V_{mp}, I_{mp}, at SRC, and coefficients $\mu_{V,oc}$ and $\mu_{I,sc}$. Resistances R_{so} and R_{sho} can only be obtained from the graphical data, when they are provided by the manufacturers.

As it is resumed by Sloplaki et al. [19], several authors have proposed by many simplified correlations for predicting the electrical performance of a PV module; these relations, that do not use five or seven-parameter models, especially emphasize the role of the conversion efficiency. It is well known the expression (3) proposed by Evans [20] to describe the module's efficiency η in correspondence of given values of temperature T and solar irradiance G:

$$\eta = \eta_{ref}\left[1 - \beta(T - T_{ref}) + \delta\log_{10}\left(\frac{G}{G_{ref}}\right)\right] \quad (3)$$

where η_{ref} is the efficiency at SRC. Temperature coefficient β and solar radiation coefficient δ have values of 0.004 K^{-1} and 0.12, respectively, for crystalline silicon modules [21]. Using the expression (4) proposed by Kou et al. [22], and observing that the efficiency is much smaller than the product of the glazing solar transmittance and the PV panel solar absorptance [23], the silicon temperature, which is not readily available, can be replaced by the nominal operating cell temperature T_{NOCT}:

$$\eta = \eta_{ref}\left\{1 - \beta\left[T_a - T_{ref} + (T_{NOCT} - T_a)\frac{G}{G_{NOCT}}\right]\right\} \quad (4)$$

In Eq. (4) T_a is the ambient temperature and G_{NOCT} (800 W/m^2) is the irradiance used in defining T_{NOCT}. Other correlations [24–27] use empirical constants whose values are only provided for few models of PV panels.

Simple correlations like Eqs. (3) and (4), which try to represent the general behaviour of any unspecified PV panel, are useful only if a first approach to the energy assessment of a photovoltaic system is required. Adversely, five or seven parameter models, which give a very accurate description of the electrical behaviour of a PV panel, require much specific information on the performance data of the studied device; unfortunately, the required wide set of information is not provided by all manufacturers. Manufacturers always provide tabular performance data, referred to SRC, that describe the voltage and the current at the maximum power, open circuit voltage and short circuit current; open circuit voltage, short circuit current and maximum power temperature coefficients are also provided to take account of working conditions far from SRC.

The few above data are used by PVsyst [28], which is a well-known PC software package for the study, sizing, simulation and data analysis of complete PV systems. PVsyst is endowed with a database of components that contains the performance tabular data provided by a huge number of manufactures. A PV panel is analytically described by means of the following one-diode equation:

$$I = I_L - I_0\left(e^{\frac{q\,(V+IR_s)}{N_{cs}\gamma kT}} - 1\right) - \frac{V + IR_s}{R_{sh}} \quad (5)$$

The parameters I_L, I_0 and R_s are determined by solving a system of three equations that satisfy the conditions under which Eq. (5) contains the short circuit, the open circuit and any other point, close the maximum power point. As it is issued in the PVsyst contestual help, the ideality factor γ is set at a reasonable level depending on the semiconductor material (γ = 1.30 for Si-monocrystalline, γ = 1.35 for Si-polycrystalline) and for N_{cs}, which is the number of cells connected in series, the value provided by the manufacture is used. Resistance R_{sh}, which is assumed to be the inverse of the slope of the *I–V* characteristic in the neighbourhood of the short circuit point, is determined by calculating the so-called virtual maximum power point conductance $(I_{sc} - I_{mp})/V_{mp}$, corresponding to the minimum value for $R_{sh,}$ and taking a given fraction of this quantity. Shunt resistance R_{sh} is considered to be variable with the irradiance according to the following exponential expression:

$$R_{sh}(G) = R_{sh} + [R_{sh}(0) - R_{sh}]e^{-5.5G/G_{ref}} \quad (6)$$

that was derived by observing the behaviour of all the analysed PV panels. For silicon crystalline modules, resistance $R_{sh}(0)$ is set to the default value of four times R_{sh}. The default value, which was deduced from measurements on six PV modules, is not considered very reliable by the authors of PVsyst. The used model gives an accurate representation of the *I–V* characteristics of PV panels. Unfortunately it is almost impossible to use the PVsyst model out of the original software because the given fraction of the so-called virtual maximum power point conductance and the equations necessary to evaluate the model parameters are not explicitly provided.

A different approach to the problem has been recently adopted by Saloux et al. [17] to write a set of equations based on the single-diode model of Eq. (5). Series and shunt resistances are neglected and four equations are written for the short circuit, the open circuit point and the maximum power point of the *I–V* characteristic. Considering the asymptotic behaviour of the *I–V* curve at short and open circuit conditions, the derivative of the current in correspondence of the maximum power is calculated as:

$$\frac{dI}{dV}\Big|_{V_{mp}} \cong -\frac{I_{sc}}{V_{oc}} \tag{7}$$

Photocurrent I_L, ideality factor γ and reverse saturation current I_0 are calculated with the following equations:

$$I_L = \frac{G}{G_{ref}}[I_{sc} + \mu_{I,sc}(T - T_{ref})] \tag{8}$$

$$\gamma = -\frac{q(V_{mp} - V_{oc})}{N_{cs}kT}\left[\ln\left(1 - \frac{I_{mp}}{I_{sc}}\right)\right]^{-1} \tag{9}$$

$$I_0 = \frac{I_{sc} + \mu_{I,sc}(T - T_{ref})}{e^{\frac{q[(V_{oc}+\mu_{V,oc}(T-T_{ref})]}{N_{cs}\gamma kT}} - 1} \tag{10}$$

For high solar irradiances the Saloux et al. model is considered quite accurate. However, the open circuit voltage at low solar irradiances is underestimated; this is supposed to be principally due to the high value of the ideality factor calculated with Eq. (9). In the opinion of Saloux et al., series and parallel resistances do not strongly affect the behaviour of the *I–V* characteristic curve.

3. A new model based on tabular performance data

Both PVsyst and Saloux et al. models have the merit of using only the tabular performance data that are the minimal information provided by all the PV panel manufacturers; nevertheless, some of the used positions seem a bit unjustified and may be avoided or changed in order to get a better accuracy.

The one-diode Lo Brano et al. [16] model accurately describes the *I–V* characteristic of a PV panel with the following equation:

$$I(\alpha_G, T) = \alpha_G I_L(T) - I_0(\alpha_G, T)\left(e^{\frac{\alpha_G[V + K\,I(T - T_{ref})] + I\,R_s}{\alpha_G nT}} - 1\right) - \frac{\alpha_G[V + K\,I(T - T_{ref})] + IR_s}{R_{sh}} \tag{11}$$

where the quantity $\alpha_G = G/G_{ref}$ denotes the ratio between the generic solar irradiance and the solar irradiance at SRC. K is a thermal correction factor similar to the curve correction factor described by the IEC 891. The model requires the knowledge of V_{oc}, I_{sc}, V_{mp}, I_{mp}, R_{so} and R_{sho} at SRC, and coefficients $\mu_{V,oc}$ and $\mu_{I,sc}$. To get the best representation of the *I–V* characteristic the open circuit voltage at $G \neq G_{ref}$ and $T = T_{ref}$; and the voltage and current at the maximum power point at $G = G_{ref}$ and $T \neq T_{ref}$, are used.

The approach to the determination of the values of the parameters contained in Eq. (2) is traditionally based on defining and solving a suitable system of equations. Lo Brano et al. adopted a very effective method consists in using five equations: three equations satisfy the conditions for which Eq. (11) contains the short circuit, the open circuit and maximum power points; two equations set the derivative of Eq. (11) in correspondence of the short circuit and the open circuit points equal to the slopes of the characteristic curve in these points. Such a model requires some information that can only be extracted from the *I–V* curves issued by the manufacturers.

In this paper a new procedure based on the performance tabula data is presented. The procedure uses an approximate solution of the following equations that are referred to the short circuit point ($I = I_{sc}$; $V = 0$) at SRC:

$$I_{sc} = I_L - I_0\left(e^{\frac{I_{sc}R_s}{nT}} - 1\right) - \frac{I_{sc}R_s}{R_{sh}} \tag{12}$$

$$\frac{dI}{dV}\Big|_{\substack{V=0\\I=I_{sc}}} = -\frac{\frac{I_0}{nT}e^{\frac{I_{sc}R_s}{nT}} + \frac{1}{R_{sh}}}{1 + R_s\left[\frac{I_0}{nT}e^{\frac{I_{sc}R_s}{nT}} + \frac{1}{R_{sh}}\right]} = -\frac{1}{R_{sho}} \tag{13}$$

It is easy to verify that under the positions:

$$I_0\left(e^{\frac{I_{sc}R_s}{nT}} - 1\right) \ll I_LR_s \ll R_{sh}\frac{I_0}{nT}e^{\frac{I_{sc}R_s}{nT}} \ll \frac{1}{R_{sh}} \tag{14}$$

Eqs. (12) and (13) yield the following approximate values of photocurrent I_L and shunt resistance R_{sh}:

$$I_L \cong I_{sc} \quad R_{sh} \cong R_{sho} \tag{15}$$

In order to prove that the above positions are acceptable and correspond to physically possible conditions, Table 1 lists the values of I_{sc}, I_0, nT, I_L, R_s and R_{sh} of some PV panels at SRC. For each panel the parameters of the corresponding one-diode equivalent circuit were calculated with the procedure described in [16]; such a procedure determines the parameters with a very high degree of accuracy without using any approximate equation.

Table 1 shows that, although the values of I_{sc}, I_0, nT, I_L, R_s and R_{sh} are quite different for each panel, the positions of Eqs. (14) are always greatly satisfied. Table 2 allows the comparison between I_{sc}, I_L, R_{sho} and R_{sh}; as expected, the differences between the values I_{sc} and R_{sho} found in the *I–V* characteristics and the values of I_L and R_{sh} calculated with the procedure described in [16] are quite negligible.

Because the evaluation of I_L and R_{sh} can be avoided, only three parameters of the one-diode equivalent circuit must be calculated. To determine the values of I_0, n, and R_s at SRC the following equations can be used:

$$0 = I_{sc} - I_0\left(e^{\frac{V_{oc}}{nT}} - 1\right) - \frac{V_{oc}}{R_{sho}} \tag{16}$$

$$\frac{dI}{dV}\Big|_{\substack{V=V_{oc}\\I=0}} = -\frac{\frac{I_0}{nT}\,e^{\frac{V_{oc}}{nT}} + \frac{1}{R_{sho}}}{1 + R_s\left[\frac{I_0}{nT}\,e^{\frac{V_{oc}}{nT}} + \frac{1}{R_{sho}}\right]} = -\frac{1}{R_{so}} \tag{17}$$

$$I_{mp} = I_{sc} - I_0\left(e^{\frac{V_{mp}+I_{mp}R_s}{nT}} - 1\right) - \frac{V_{mp} + I_{mp}R_s}{R_{sho}} \tag{18}$$

Table 1
Numerical verification of the positions of Eq.(14).

Panel type	I_{sc} (A)	I_0 (A)	nT (V)	R_s (Ω)	R_{sh} (Ω)	$I_0\left(e^{\frac{I_{sc}R_s}{nT}} - 1\right)$ (A)	I_L (A)	$\frac{I_0}{nT}e^{\frac{I_{sc}R_s}{nT}}$ (Ω^{-1})	$1/R_{sh}$ (Ω^{-1})
Canadian CS5P-250 M	5.47	1.79×10^{-10}	2.36	0.33	647.17	2.05×10^{-10}	5.46	1.63×10^{-10}	1.55×10^{-3}
Photowatt PW6-123	7.47	7.07×10^{-9}	1.06	0.18	63.81	1.82×10^{-8}	7.49	2.39×10^{-8}	1.57×10^{-2}
Sanyo HIP- 215NKHE1	5.60	3.98×10^{-17}	1.30	1.27	2285.40	9.23×10^{-15}	5.61	7.11×10^{-15}	4.38×10^{-4}
Yocasol PCA 200	8.70	7.57×10^{-8}	1.77	0.29	924.86	2.40×10^{-7}	8.71	1.78×10^{-7}	1.08×10^{-3}

Table 2
Comparison between I_{sc}, I_L, R_{sho} and R_{sh}.

Panel type	I_{sc} (A)	I_L (A)	$\frac{I_{sc}-I_L}{I_L}$ (%)	R_{sho} (Ω)	R_{sh} (Ω)	$\frac{R_{sho}-R_{sh}}{R_{sh}}$ (%)
Canadian CS5P-250 M	5.47	5.46	0.183	647.50	647.17	0.051
Photowatt PW6-123	7.47	7.49	−0.267	63.99	63.81	0.282
Sanyo HIP- 215NKHE1	5.60	5.61	−0.178	2,286.67	2,285.40	0.056
Yocasol PCA 200	8.70	8.71	−0.115	925.00	924.86	0.015

in which I_L and R_{sh} were substituted by I_{sc} and R_{sho}, respectively. Eqs. (16) and (18) satisfy the conditions under which Eq. (11) contains the open circuit and maximum power points at SRC; Eq. (17) sets the derivative of Eq. (11) in correspondence of the open circuit point equal to the slope of the characteristic curve in this point. Eq.(16) yields:

$$I_0 = \frac{I_{sc} - V_{oc}/R_{sho}}{e^{\frac{V_{oc}}{nT}} - 1} \tag{19}$$

that can be substituted in Eq. (18) in order to obtain:

$$n = \frac{V_{mp} + I_{mp}R_s - V_{oc}}{T}\left[\ln\left(\frac{(I_{sc} - I_{mp})R_{sho} - (V_{mp} + I_{mp}R_s)}{I_{sc}R_{sho} - V_{oc}}\right)\right]^{-1} \tag{20}$$

The exponential terms in Eqs. (16) and (18) were assumed much greater than 1; such a hypothesis is always greatly verified.

Once the initial value for R_s is set in Eq. (20), n can be calculated and used to evaluate current I_0 by Eq. (19). These values of n and I_0 are then substituted in Eq. (17) to check if it is satisfied. If Eq. (17) does not result satisfied, R_s is appropriately changed and the trial and error process is reiterated until Eq. (17) is satisfied with the desired accuracy. Appendix B lists a simple BASIC computer routine that is capable of solving the system of equations according to the procedure described above; the routine can be easily implemented, even like VBA macros in Microsoft Excel.

The root-finding algorithm is a modified version of the bisection method, which is very simple and robust. To increase the reliability of the automatic procedure, the input data V_{oc}, I_{sc}, V_{mp}, I_{mp}, R_{so} and R_{sho} were range-scaled to delimit each I–V characteristic between the unity values of voltage and current. Range-scaling was achieved by dividing the voltage data by V_{oc}, the current data by I_{sc} and the resistance data by the ratio of V_{oc} and I_{sc}. Range-scaling the data permits the univocal definition of the numerical parameters that are involved in the root-finding procedure; in this way, first-attempt values such as the width of the searching interval, the bisection step and the accuracy level, which are crucial points for the bisection method, do not need to be adjusted for each PV panel.

To calculate the values of I_0, n, and R_s at SRC the values of R_{so} and R_{sho} are necessary; indeed the information regarding R_{so} and R_{sho} is never contained in the provided tabular data. To skirt the obstacle the I–V characteristics of 144 models of PV panels issued on the Internet by 30 manufacturers were surveyed. The reciprocal of slopes of the I–V curve in correspondence of the short circuit and open circuit points correspond to R_{sho} and R_{so}, respectively; in Fig. 2 the rules of the approximate procedure used to get the values of R_{sho} and R_{so}, are depicted.

The range-scaled values of R_{so} and R_{sho} extracted from the measured characteristics are listed in Table A1 of Appendix A. It was observed that both R_{so} and R_{sho} can be reasonably represented by means of the following relations:

$$R_{so} = C_s\frac{V_{oc}}{I_{sc}} \quad R_{sho} = C_{sh}\frac{V_{oc}}{I_{sc}} \tag{21}$$

with C_s = 0.11175 and C_{sh} = 34.49692. For PV panels based on the Sanyo HIT (heterojunction with intrinsic thin layer) technology

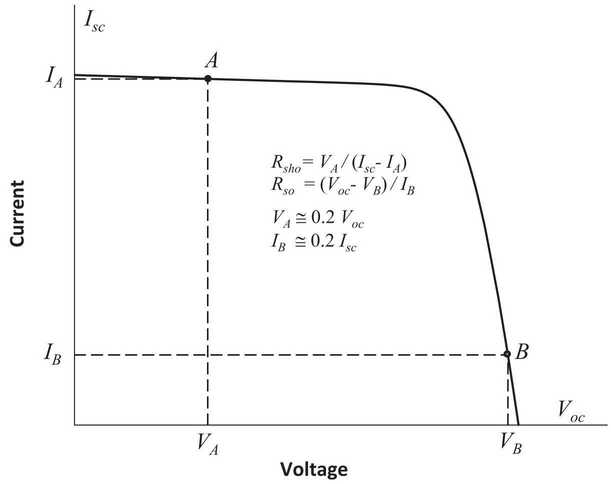

Fig. 2. Graphical evaluation of Rso and R_{sho} in the I–V characteristic at SRC.

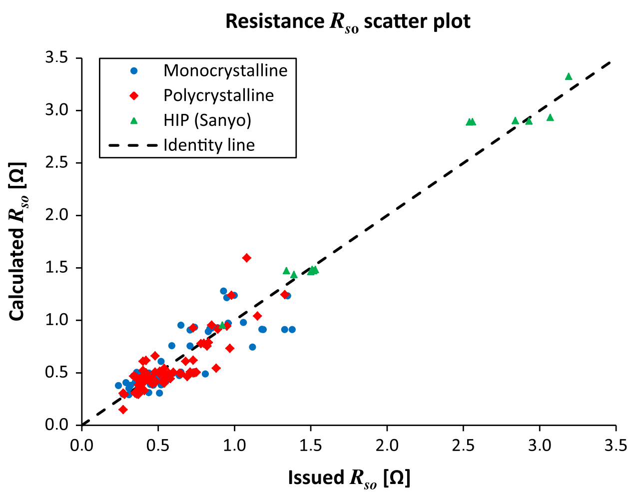

Fig. 3. Comparison between the calculated values of R_{so} and the values extracted from I–V characteristic at SRC.

different values of coefficients C_s and C_{sh} have to be used; suitable values are C_s = 0.16129 and C_{sh} = 124.48114. Figs. 3 and 4 illustrate the correspondence between the values of R_{so} and R_{sho} extracted from the I–V characteristics and the values calculated with Eq. (21). In the x-axis of Figs. 3 and 4 the values of R_{so}, or R_{sho}, extracted from the characteristics issued by the manufacturers, are reported; in the y-axis the calculated ones are indicated.

Because a point on the identity line corresponds to a perfect correspondence between issued and calculated values, the markers lying under the identity line indicate calculated values that are smaller than the values extracted from the issued characteristics; the opposite is for the values represented by the markers that are over the identity line. The Pearson correlation coefficient assumes the values of 0.84 for R_{so} and 0.86 for R_{sho}, which indicate

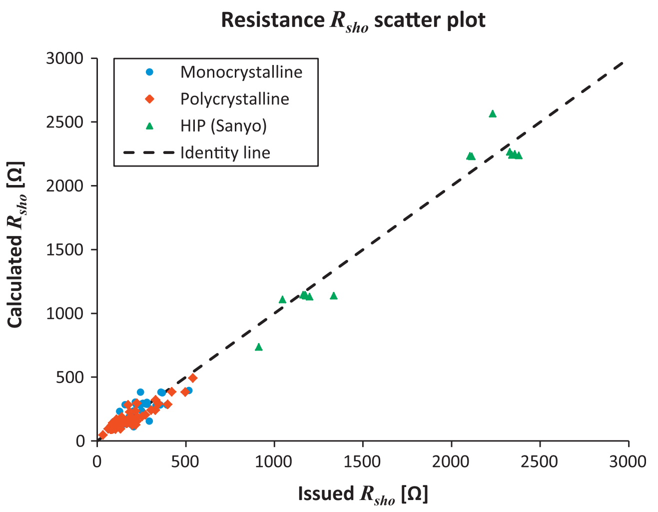

Fig. 4. Comparison between the calculated values of R_{sho} and the values extracted from I–V characteristic at SRC.

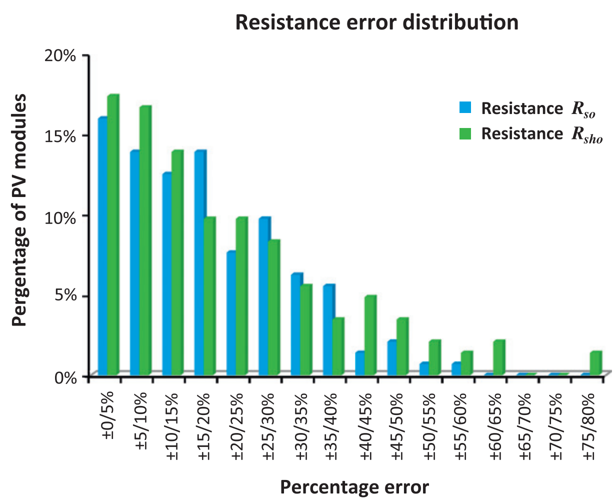

Fig. 5. Histogram of the percentage of panels versus the percentage error of the values of R_{so} and R_{sho} calculated with Eq. (21).

a strong correlation between issued and calculated values. In Fig. 5 the distribution of the percentage error due to the use of Eq. (21) is depicted.

An error less than 25% affects resistances R_{so} calculated for 73.6% of the surveyed I–V characteristics; an analogous maximum error affects the calculations of R_{sho} performed for 67.4% of the analysed PV panels. For mono crystalline and polycrystalline panels the root mean square errors in evaluating R_{so} and R_{sho} are 0.15 Ω and 49.51 Ω, respectively; for the HIP panels the analogous root mean square errors are 0.25 Ω and 138.62 Ω.

The reverse saturation current $I_0(\alpha_G,T)$ can be calculated by means of the following Eq. (22) that is derived from the equation that satisfies the condition under which Eq. (11) contains the open circuit point of the I–V characteristic at given values of irradiance G and temperature T.

$$I_0(\alpha_G,T)=\alpha_G\left(\frac{I_L(T)-V_{oc}(\alpha_G,T)/R_{sho}}{e^{\frac{V_{oc}(\alpha_G,T)}{nT}}-1}\right) \tag{22}$$

In order to take account of the dependence of the photocurrent on the temperature, the following expression is used:

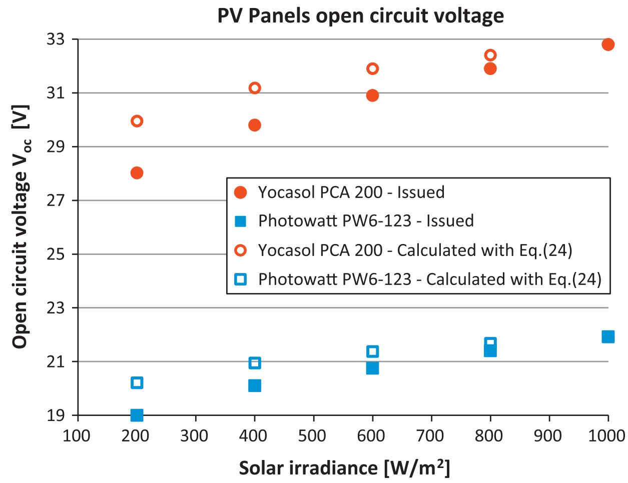

Fig. 6. Comparison between the values of the open circuit voltage evaluated with Eq. (24), at various irradiances and T = 25 °C, and the values issued by the manufacturers.

$$I_L(T)=I_{sc}+\mu_{I,sc}(T-T_{ref}) \tag{23}$$

For the evaluation of $V_{oc}(\alpha_G,T)$, Celik et al. [13] and Hadj Arab et al. [15] used the following expression proposed by Chenlo et al. [29]:

$$V_{oc}(\alpha_G,T)=V_{oc,ref}+nT\ln\left(\frac{G}{G_{ref}}\right)+\mu_{V,oc}(T-T_{ref}) \tag{24}$$

The above expression, is quite imprecise because was obtained from Eq. (2) on the basis of the simplified hypotheses of the four-parameter model, in which it is $R_{sh}=\infty$. Moreover, when the irradiance tends to zero, Eq. (24) yields an unrealistic value of the open circuit voltage ($V_{oc}\to-\infty$). In Fig. 6 the values of V_{oc}, calculated with Eq. (24) using the data of Table 1, are depicted; for an irradiance of 200 W/m^2, Eq. (24) evaluates the open circuit voltage of the Yocasol PCA 200 and the Photowatt PW6-123 panels with an error of 1.93 V and 1.21 V, respectively.

In order to get a more accurate description of $V_{oc}(\alpha_G,T)$, the I–V characteristics of 108 models of PV panels issued on the Internet by 23 manufacturers were surveyed. For each panel the values of V_{oc} at the various irradiances were collected; Table A2 of the Appendix A lists the values of the open circuit voltage for each PV panel. Some data of the Table A2 are missing because some issued I–V characteristics were incompletely drawn. From the analysis of the scaled values of V_{oc} resulted that a good accuracy can be achieved using the following interpolating relation:

$$V_{oc}(\alpha_G)=V_{oc,ref}+\{C_1\ln(\alpha_G)+C_2[\ln(\alpha_G)]^2+C_3[\ln(\alpha_G)]^3\}+\mu_{V,oc}(T-T_{ref}) \tag{25}$$

where $C_1=5.468511\times10^{-2}$, $C_2=5.973869\times10^{-3}$ and $C_3=7.616178\times10^{-4}$. The goodness of fit is shown in Fig. 7. The interpolating curve tries to best fit the mean values of the measured V_{oc} at the various irradiances.

For $G=1000$ W/m^2 and that $T=T_{ref}$, Eq. (25) correctly yields $V_{oc}=V_{oc,ref}$. To avoid the miscalculation of V_{oc} in correspondence of values of the irradiances smaller than 200 W/m^2, the interpolating curve contains the origin of the diagram as it is shown in Fig. 8.

As a matter of fact, the presence of the logarithms in Eq. (25) does not permit to set $\alpha_G=0$; for this reason the coefficients were determined by imposing that the interpolating curve contains a point that is very close to the origin ($\alpha_G=0.01$). The accuracy obtained with Eq. (25) is evident in Fig. 9 in which it is possible to observe the dispersion of the measured and calculated values of the open circuit voltage for all PV panels and all values of the

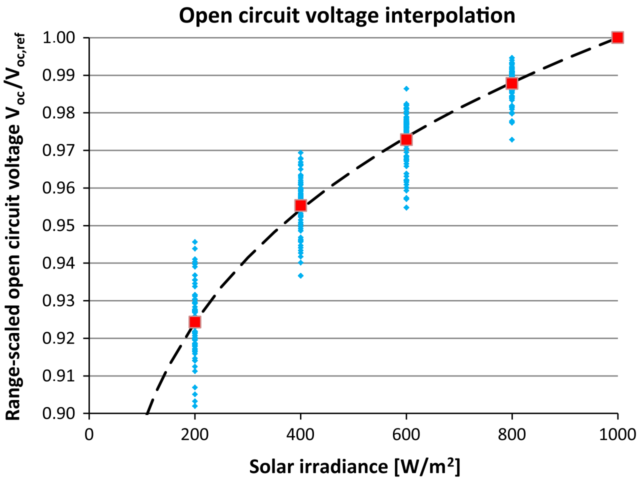

Fig. 7. Interpolation of the mean values (squares) of the range scaled values of V_{oc} at various irradiances and T = 25 °C.

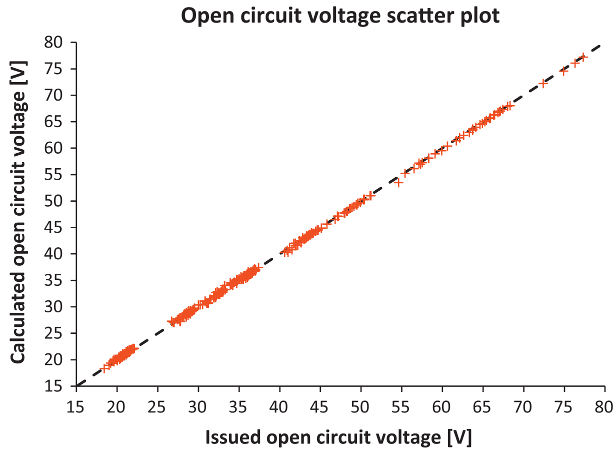

Fig. 9. Dispersion of the measured and calculated values of the open circuit voltage at T = 25 °C.

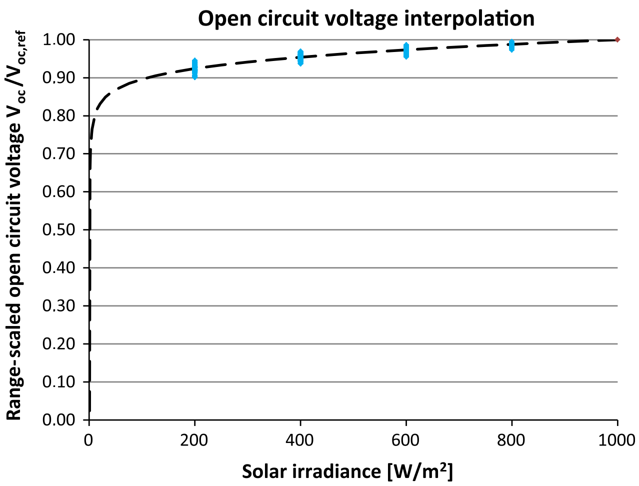

Fig. 8. Interpolation range scaled open circuit voltage at T = 25 °C.

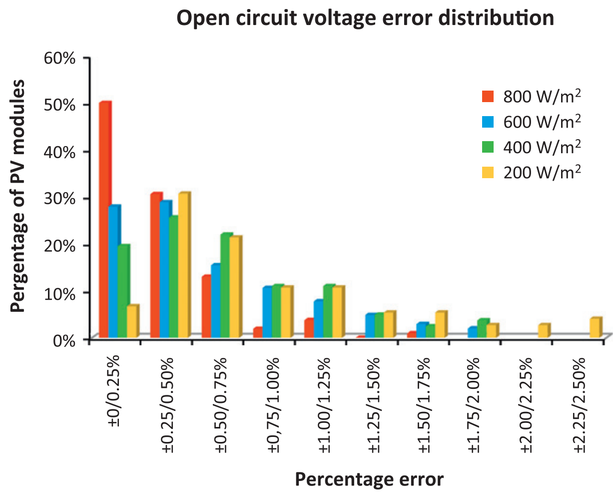

Fig. 10. Histogram of the percentage of panels versus the percentage error of the values of V_{oc} calculated with Eq. (25).

irradiance listed in Table A2. In the x-axis values of V_{oc} extracted from the characteristics issued by the manufacturers are reported; in the y-axis the calculated ones are indicated.

The Pearson correlation coefficient is of 0.9999, which indicate a very strong correlation between issued and calculated values. The distribution of the error is shown in the histogram of Fig. 10 in which, for each value of the irradiance, the percentage of panels versus the percentage error is indicated.

Whatever the irradiance is, the error is less than 1% and 2% for 69.3% and 93.3% of PV panels, respectively; the root mean square error is 0.24 V. By substituting Eq. (25) in Eq. (22) it is possible to directly calculate the value of the reverse saturation current $I_0(\alpha_G,T)$.

Thermal correction factor K of Eq. (11) permits to improve the performance of the model for temperatures different from SRC. The effect of K is to slide the I–V characteristic curve at irradiance G_{ref} along the V axis to better fit the characteristics provided by the manufacturer for temperatures different from T_{ref}. When maximum power temperature coefficient $\mu_{P,max}$ is provided by the manufacturer, it is possible to calculate coefficient K by imposing that the maximum power calculated with Eq. (11) at $G = 1000\ \text{W/m}^2$ and $T = T^* \neq 25$ °C corresponds to the maximum power evaluated by means of coefficient $\mu_{P,max}$. To set such a correspondence it necessary to find the maximum of power P^* generated at $\alpha_G = 1$ and $T = T^*$:

$$P^* = V^* I^* = V\left[I_L^* - I_0^*\left(e^{\frac{V^*+K I^*(T^*-T_{ref})+I^* R_s}{nT^*}} - 1\right) - \frac{V^* + K I^*(T^* - T_{ref}) + I^* R_s}{R_{sho}}\right] \quad (26)$$

in which the asterisk indicates the values of the voltage, current, photocurrent and reverse saturation current referred to $\alpha_G = 1$ and $T = T^* \neq 25$ °C.

The method of Lagrange multipliers can be used for finding the maximum and minimum points of a function like Eq. (26) that is subject to a constraint like Eq. (11). The power generated by the PV panel can be rewritten in the following form:

$$P^* = V_d I^* - I^{*2} R_s \quad (27)$$

where:

$$V_d = V^* + K I^*(T^* - T_{ref}) + I^* R_s \quad (28)$$

is the voltage across the diode. Power P^*, which depends on V_d and I^*, is subject to the following constraint:

Table 3
Data for the evaluation of the new model parameters.

Panel type	V_{oc} (V)	I_{sc} (A)	V_{mp} (V)	I_{mp} (A)	$\mu_{V,oc}$ (V/°C)	$\mu_{I,sc}$ (A/°C)	$\mu_{P,max}$ (%/°C)
Gruposolar GS601456P-218	36.30	8.19	29.00	7.55	-1.27×10^{-1}	1.68×10^{-3}	−0.26
Kyocera KC175GHT-2	29.35	8.07	23.60	7.57	-1.07×10^{-1}	2.22×10^{-3}	−0.49
Sanyo HIP-230 HDE1	42.46	7.26	34.00	6.87	-1.09×10^{-1}	2.87×10^{-3}	−0.31
Shell S75	21.55	4.70	17.5	4.32	-7.14×10^{-2}	1.64×10^{-3}	−0.48

Table 4
Evaluated model parameters.

Panel type	I_L (A)	I_0(A)	n (V/K)	R_{sh} (Ω)	R_s (Ω)	K (Ω/°C)
Gruposolar GS601456P-218	8.19261	1.83598×10^{-8}	6.12215×10^{-3}	152.850	0.266	-1.62000×10^{-3}
Kyocera KC175GHT-2	8.06980	8.45857×10^{-11}	3.89833×10^{-3}	125.466	0.258	1.05827×10^{-3}
Sanyo HIP-230 HDE1	7.25665	1.50344×10^{-19}	3.14269×10^{-3}	728.362	0.814	-4.50044×10^{-4}
Shell S75	4.69484	6.45613×10^{-10}	3.18721×10^{-3}	158.346	0.305	2.40786×10^{-3}

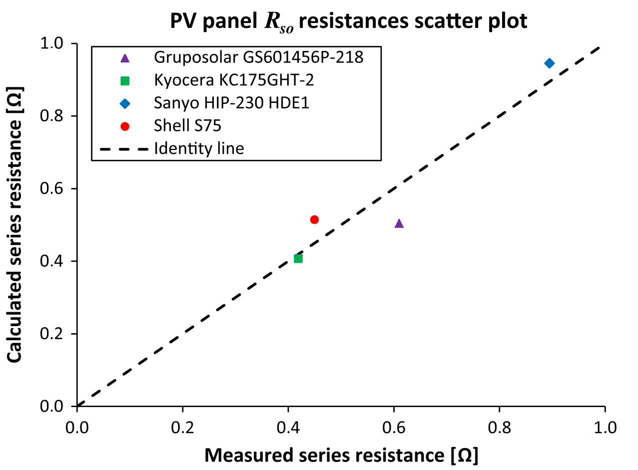

Fig. 11. Comparison between the calculated values of R_{so} and the values extracted from I–V characteristic at SRC.

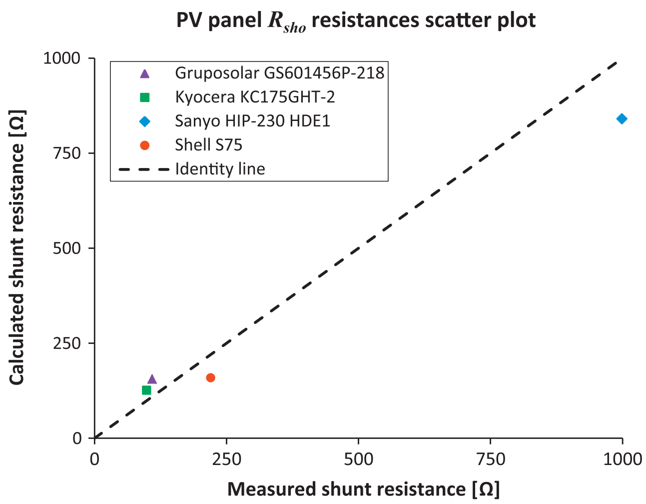

Fig. 12. Comparison between the calculated values of R_{sho} and the values extracted from I–V characteristic at SRC.

$$I^* - I_L^* + I_0^*\left(e^{\frac{V_d}{nT^*}} - 1\right) + \frac{V_d}{R_{sho}} = 0 \tag{29}$$

that is derived from Eq. (11). The application of the method of Lagrange multipliers yields the following equations:

$$\frac{\partial P^*}{\partial V_d} = I^* + \lambda\left(\frac{I_0^*}{nT^*}e^{\frac{V_d}{nT^*}} + \frac{1}{R_{sho}}\right) = 0 \tag{30}$$

$$\frac{\partial P^*}{\partial I^*} = V_d - 2I^*R_s + \lambda = 0 \tag{31}$$

where λ is a Lagrange multiplier. From Eqs. (29)–(31) the value of the voltage across the diode corresponding to the maximum power generated by the PV panel at $G = 1000\ \mathrm{W/m^2}$ and $T = T^*$ can be found:

$$V_{d,max} = nT^*\left\{\ln\left[\frac{R_{sho}(I_L^* + I_0^*) - 2(V_{d,max} - I^*R_s)}{R_{sho}(V_{d,max} - 2I^*R_s)}\right] - \ln\left[I_0^*\left(\frac{1}{nT^*} + \frac{1}{V_{d,max} - 2I^*R_s}\right)\right]\right\} \tag{32}$$

The implicit form of Eq. (32) can be easily calculated observing that the argument of the first logarithm is much smaller than the argument of the second logarithm and that the first term of the argument of the second logarithm is greater than the second term. These observations permit to calculate a first attempt value of $V_{d,max}$:

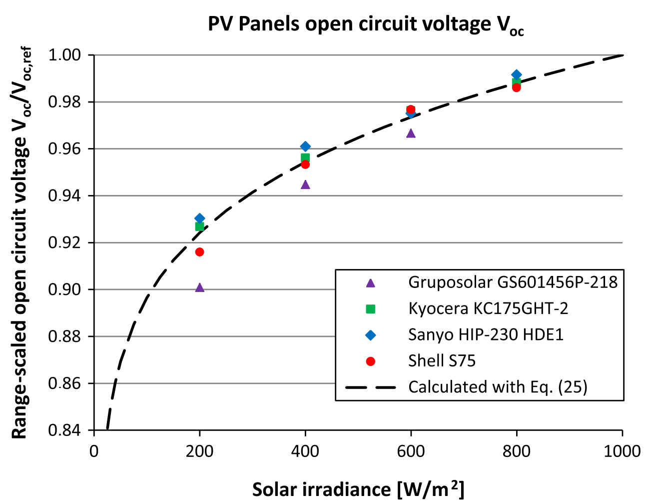

Fig. 13. Comparison between the calculated values of V_{oc} and the values extracted from I–V characteristic at SRC.

$$V_{d,max} \cong -nT^* \ln\left(\frac{I_0^*}{nT^*}\right) \tag{33}$$

that can be substituted in Eq. (32) to start calculations. The calculated value of $V_{d,max}$ is again substituted in Eq. (32), and after few

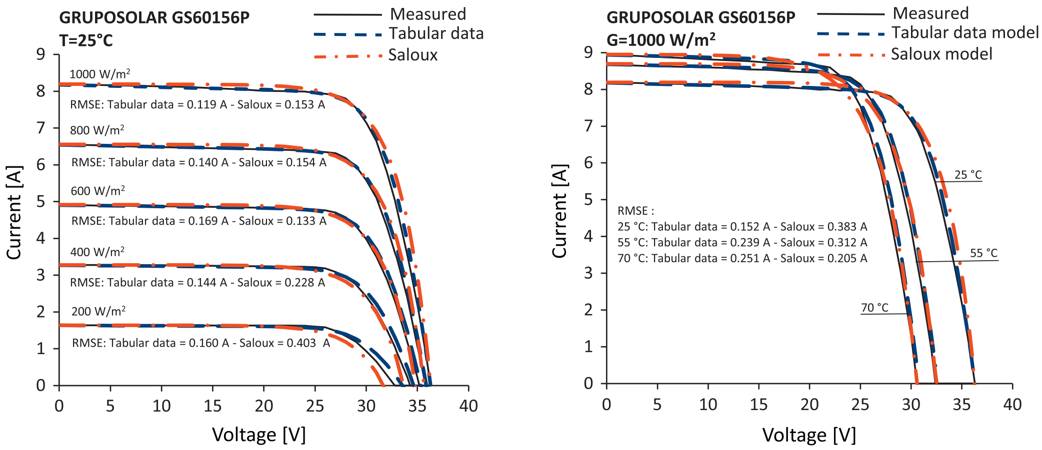

Fig. 14. Comparison between the measured *I–V* characteristics of Gruposolar GS60156P and the characteristics calculated with the Saloux et al. and the Tabular data models.

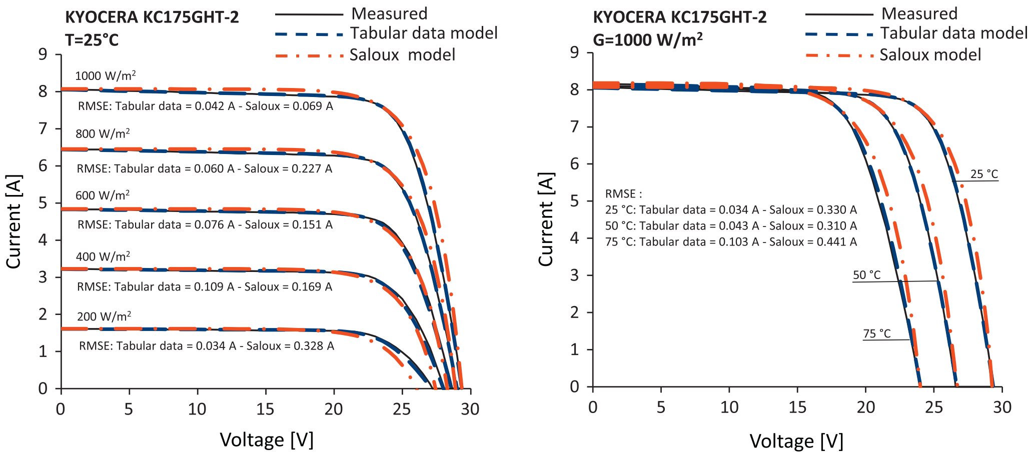

Fig. 15. Comparison between the measured *I–V* characteristics of Kyocera KC175GHT-2 and the characteristics calculated with the Saloux et al. and the Tabular data models.

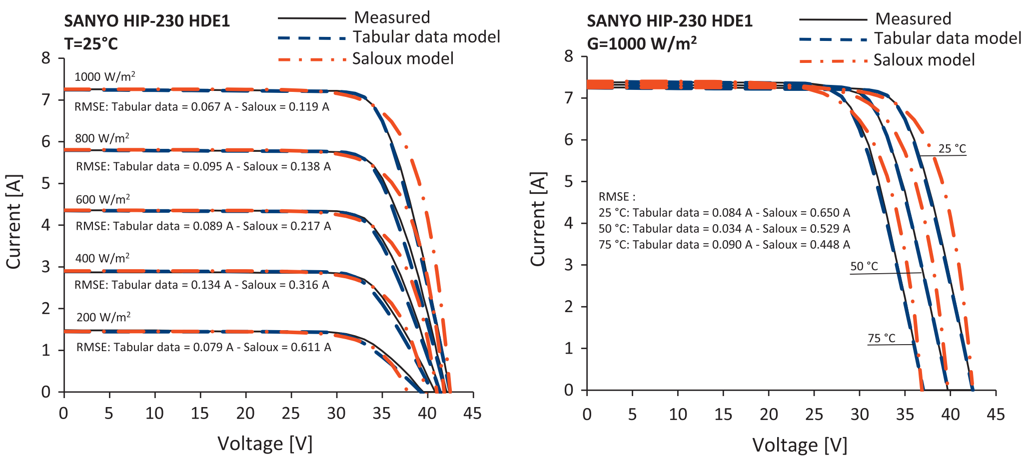

Fig. 16. Comparison between the measured *I–V* characteristics of Sanyo HIP-230 HDE1 and the characteristics calculated with the Saloux et al. and the Tabular data models.

iterations a stable value of $V_{d,max}$ can be obtained. The values of current I^*_{max} and voltage V^*_{max} corresponding with the maximum power point at G = 1000 W/m^2 and $T = T^*$ can be derived from Eqs. (28) and (29):

$$I^*_{max} = I^*_L - I^*_0\left(e^{\frac{V_{d,max}}{nT^*}} - 1\right) - \frac{V_{d,max}}{R_{sho}} \tag{34}$$

$$V^*_{max} = V_{d,max} - K I^*_{max}(T^* - T_{ref}) - I^*_{max}R_s \tag{35}$$

The required value of maximum power P^*_{max} is given by:

$$P^*_{max} = V^*_{max}I^*_{max} = V_{d,max} - K I^*_{max}(T^* - T_{ref}) + I^* R_s \tag{36}$$

Once an initial value for the thermal correction factor K is set in Eq. (28), maximum power P^*_{max} is calculated with the above procedure and used to verify the following equation:

$$P^*_{max} = P_{max}\left[1 + \frac{\mu_{P,max}}{100}(T^* - T_{ref})\right] \tag{37}$$

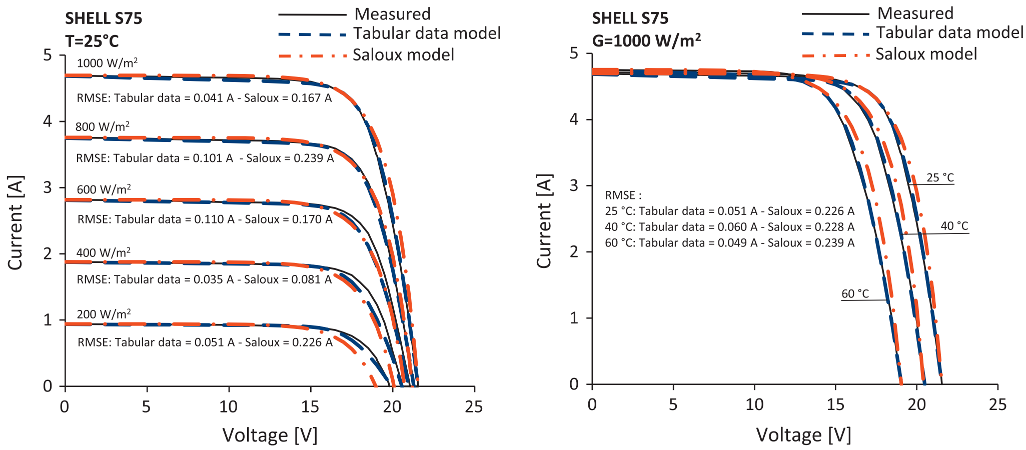

Fig. 17. Comparison between the measured *I–V* characteristics of Shell S75 and the characteristics calculated with the Saloux et al. and the Tabular data models.

Table 5
Maximum current differences between the measured and the calculated current and voltage at temperature *T* = 25 °C. Alex.

Parameters at the maximum difference points			Irradiance (W/m²)				
			200	400	600	800	1000
Gruposolar GS601456P-218	Tabular data model	Voltage (V)	32.00	33.00	34.00	32.80	34.00
		Measured Current (A)	0.285	0.902	1.187	3.621	3.562
		Calc. Current (A)	0.567	1.189	1.487	3.944	3.951
		Difference (A)	**0.282**	**0.287**	**0.300**	**0.323**	**0.389**
	Saloux model	Voltage (V)	31.00	33.00	32.80	32.80	34.00
		Measured Current (A)	0.653	0.902	2.303	3.621	3.562
		Calc. Current (A)	0.350	0.687	2.501	4.139	4.521
		Difference (A)	**−0.303**	**−0.215**	**0.198**	**0.518**	**0.959**
Kyocera KC175GHT-2	Tabular data model	Voltage (V)	26.00	27.00	27.00	26.00	26.50
		Measured Current (A)	0.628	1.106	2.288	4.621	5.430
		Calc. Current (A)	0.516	0.931	2.081	4.584	5.538
		Difference (A)	**−0.112**	**−0.175**	**−0.207**	**−0.037**	**0.108**
	Saloux model	Voltage (V)	26.00	27.20	28.06	27.20	28.06
		Measured Current (A)	0.628	0.905	0.847	3.117	2.891
		Calc. Current (A)	0.012	0.370	0.513	3.597	3.740
		Difference (A)	**−0.616**	**−0.535**	**−0.334**	**0.480**	**0.849**
Sanyo HIP-230 HDE1	Tabular data model	Voltage (V)	36.00	38.00	37.00	39.00	39.50
		Measured Current (A)	0.801	1.230	2.804	2.747	3.233
		Calc. Current (A)	0.658	1.034	2.572	2.406	3.014
		Difference (A)	**−0.143**	**−0.196**	**−0.232**	**−0.341**	**−0.219**
	Saloux model	Voltage (V)	37.00	39.50	38.00	39.50	40.00
		Measured Current (A)	0.601	0.601	2.232	2.289	2.690
		Calc. Current (A)	0.352	0.294	2.801	3.197	4.156
		Difference (A)	**−0.249**	**−0.307**	**0.569**	**0.908**	**1.466**
Shell S75	Tabular data model	Voltage (V)	18.50	19.05	19.50	19.05	19.50
		Measured Current (A)	0.577	1.221	1.690	2.746	3.005
		Calc. Current (A)	0.475	1.001	1.472	2.656	3.128
		Difference (A)	**−0.102**	**−0.220**	**−0.218**	**−0.09**	**0.123**
	Saloux model	Voltage (V)	18.50	20.00	20.60	20.00	20.60
		Measured Current (A)	0.577	0.516	0.540	1.784	1.620
		Calc. Current (A)	0.238	0.092	0.221	1.970	2.099
		Difference (A)	**−0.339**	**−0.424**	**−0.319**	**0.186**	**0.479**

The bold highlights the results; 0.389 is the maximum current difference value for tabular data model; 1.466 is the maximum current difference value for Saloux model.

where P_{max} is the maximum power at SRC. If Eq. (37) does not result satisfied, K is appropriately changed and the trial and error process is reiterated until Eq. (37) is satisfied with the desired accuracy. Appendix B lists a simple BASIC computer routine that is capable of calculating thermal correction factor K according to the procedure described above; the routine can be easily implemented, even like VBA macros in Microsoft Excel. The ability of the new model to reproduce the maximum power generated by the PV panel for operating temperatures far from the SRC is a very effective skill especially when the use of inverters equipped with maximum power point trackers is assumed to predict the energy produced by a PV system.

Table 6
Maximum current differences between the measured and the calculated current and voltage at Irradiance $G = 1000\ W/m^2$. Alex.

Parameters at the maximum difference points			Temperature (°C)						
			25	40	50	55	60	70	75
Gruposolar GS601456P-218	Tabular data model	Voltage (V)	34.00	–	–	30.60	–	28.00	–
		Measured Current (A)	3.562	–	–	3.281	–	4.462	–
		Calc. Current (A)	3.951	–	–	3.811	–	5.067	–
		Difference (A)	0.389	–	–	0.530	–	**0.605**	–
	Saloux model	Voltage (V)	34.00	–	–	30.60	–	29.00	–
		Measured Current (A)	3.562	–	–	3.281	–	3.018	–
		Calc. Current (A)	4.521	–	–	3.936	–	3.441	–
		Difference (A)	**0.959**	–	–	**0.655**	–	**0.423**	–
Kyocera KC175GHT-2	Tabular data model	Voltage (V)	26.50	–	26.50	–	–	–	22.00
		Measured Current (A)	5.430	–	0.293	–	–	–	3.462
		Calc. Current (A)	5.538	–	0.410	–	–	–	3.741
		Difference (A)	**0.108**	–	0.117	–	–	–	0.279
	Saloux model	Voltage (V)	28.06	–	25.00	–	–	–	22.00
		Measured Current (A)	2.891	–	3.413	–	–	–	3.462
		Calc. Current (A)	3.740	–	4.272	–	–	–	4.602
		Difference (A)	**0.849**	–	**0.859**	–	–	–	**1.140**
Sanyo HIP-230 HDE1	Tabular data model	Voltage (V)	39.50	–	35.00	–	–	–	31.00
		Measured Current (A)	3.233	–	4.760	–	–	–	5.868
		Calc. Current (A)	3.014	–	4.628	–	–	–	5.616
		Difference (A)	−**0.219**	–	−**0.132**	–	–	–	−**0.252**
	Saloux model	Voltage (V)	40.00	–	37.00	–	–	–	34.00
		Measured Current (A)	2.690	–	2.804	–	–	–	3.162
		Calc. Current (A)	4.156	–	4.260	–	–	–	4.355
		Difference (A)	**1,466**	–	**1.456**	–	–	–	**1.193**
Shell S75	Tabular data model	Voltage (V)	19.50	19.80	–	–	16.00	–	–
		Measured Current (A)	3.005	1.286	–	–	3.571	–	–
		Calc. Current (A)	3.128	1.158	–	–	3.654	–	–
		Difference (A)	**0.123**	−**0.128**	–	–	**0.083**	–	–
	Saloux model	Voltage (V)	20.60	19.05	–	–	17.50	–	–
		Measured Current (A)	1.620	2.190	–	–	2.248	–	–
		Calc. Current (A)	2.099	2.699	–	–	2.752	–	–
		Difference (A)	**0.479**	**0.509**	–	–	**0.504**	–	–

The bold highlights the results; 0.605 is the maximum current difference value for tabular data model; 1.456 is the maximum current difference value for Saloux model.

Table 7
Absolute mean current and power differences between the measured and the calculated *I–V* characteristics at temperature $T = 25\ °C$.

PV PANEL	Absolute mean difference		Irradiance (W/m^2)				
			200	400	600	800	1000
Gruposolar GS601456P-218	Current (A)	Tabular data model	0.070	0.086	0.085	0.091	**0.100**
		Saloux model	0.074	0.059	0.068	0.155	0.260
	Power (W)	Tabular data model	2.063	2.551	2.702	2.880	**3.118**
		Saloux model	2.034	1.661	1.805	4.498	8.163
Kyocera KC175GHT-2	Current (A)	Tabular data model	0.027	0.036	0.047	0.017	0.021
		Saloux model	0.100	0.093	0.068	0.113	0.203
	Power (W)	Tabular data model	0.623	0.855	1.166	0.315	0.487
		Saloux model	2.287	2.106	1.381	2.479	4.907
Sanyo HIP-230 HDE1	Current (A)	Tabular data model	0.047	0.067	0.060	0.077	0,049
		Saloux model	0.050	0.063	0.119	0.201	**0.341**
	Power (W)	Tabular data model	1.383	2.151	2.063	2.946	1.770
		Saloux model	1.429	1.894	4.383	7.589	**13.342**
Shell S75	Current (A)	Tabular data model	0.026	0.066	0.078	0.028	0.038
		Saloux model	0.068	0.137	0.095	0.053	0.143
	Power (W)	Tabular data model	0.467	1.234	1.451	0.469	0.648
		Saloux model	1.162	2.537	1.761	0.959	2.817

The bold highlights the results; 0.100 is the absolute current difference value for tabular data model; 0.341 is the absolute current difference value for Saloux model; 3.118 is the absolute power difference value for tabular data model; 13.342 is the absolute current difference value for Saloux model.

4. Application of the procedure and analysis of the results

With the aim of verifying the effectiveness of the new model, a comparison with the Saloux et al. model was made. Both models were used for drawing the *I–V* characteristics of some crystalline silicon panels whose performance data are listed in Table 3.

For the sake of precision the data listed in Table 3 were accurately extracted from the graphs provided by manufacturers. For

Table 8
Absolute mean current and power differences between the measured and the calculated *I–V* characteristics at irradiance $G = 1000\ W/m^2$.

PV Panel	Absolute mean difference		Temperature (°C) 25	40	50	55	60	70	75
Gruposolar GS601456P-218	Current (A)	Tabular data model	0.095	–	–	0.152	–	**0.160**	–
		Saloux model	0.260	–	–	0,189	–	0,156	–
	Power (W)	Tabular data model	2.941	–	–	**4,317**	–	4,166	–
		Saloux model	8.163	–	–	4.907	–	3.453	–
Kyocera KC175GHT-2	Current (A)	Tabular data model	0.022	–	0.025	–	–	–	0.062
		Saloux model	0.203	–	0.187	–	–	–	0.251
	Power (W)	Tabular data model	0.494	–	0.529	–	–	–	1.253
		Saloux model	4.907	–	4.049	–	–	–	5.050
Sanyo HIP-230 HDE1	Current (A)	Tabular data model	0.052	–	0.020	–	–	–	0.051
		Saloux model	0.341	–	**0.281**	–	–	–	0.252
	Power (W)	Tabular data model	1.918	–	0.642	–	–	–	1.566
		Saloux model	13.342	–	**9.993**	–	–	–	8.145
Shell S75	Current (A)	Tabular data model	0.038	0.051	–	–	0.039	–	–
		Saloux model	0.143	0.146	–	–	0.144	–	–
	Power (W)	Tabular data model	0.648	0.816	–	–	0.535	–	–
		Saloux model	2.817	2.697	–	–	2.424	–	–

The bold highlights the results; 0.160 is the maximum current difference value for tabular data model; 4,317 is the maximum power difference value for tabular data model; 0.281 is the maximum current difference value for Saloux model; 9.993 is the maximum power difference value for Saloux model.

this reason some small differences with the data listed in Appendix A may be observed. Table 4 lists the values of the parameters evaluated with the new model.

Figs. 11 and 12 show the comparison between the values of R_{so} and R_{sho} extracted from the measured characteristics of the analysed PV panels and the values calculated with Eq. (21).

It easy to forecast that for the Gruposolar panel a small inaccuracy may be observed in the part of the *I–V* curve close to the open circuit point where R_{so} is extracted. Adversely, for the Sanyo panel the new model may be slightly imprecise in the part of the *I–V* curve close to the short circuit point. Fig 13 shows the comparison between the values of open circuit voltage V_{oc} extracted from the measured characteristics and the values calculated with Eq. (25). Because for the Gruposolar panel the calculated open voltage at the irradiance of 200 W/m^2 is less than the value read in the provided characteristics, the new model may underestimate open circuit voltage V_{oc} for low irradiances.

In Figs. 14–17, the current–voltage curves evaluated with both models are compared with the measured data from the manufacturer's datasheet. For each value of the irradiance, or of the temperature, the curves calculated by the new model are very close to the measured the characteristics; actually, for the highest values of the irradiance the calculated curves almost overlap the measured ones. The values of the root mean square error (RMSE) of the current, which are also reported in the figures, indicate the quality of the models.

As it was declared by the authors, the Saloux et al. model underestimates the open circuit voltage at low solar irradiances. The parallel resistance, which mainly affects the *I–V* characteristics close to the short circuit point, has a small impact; only for the Kyocera panel a small effect is observed. Adversely, the series resistance significantly impacts on the *I–V* characteristic in the zone bounded by the maximum power and the open circuit points. The presence of R_{so} is the reason why the new model is more accurate than the Saloux et al. model. For the analysed panels, Tables 5 and 6 list the maximum differences of current between the measured and the calculated data.

At a constant temperature of $T = 25$ °C, the maximum differences for current calculated by the new model and the Saloux et al. model are 0.389 and 1.466 A, respectively. If compared to the measured values of current at the maximum power point with $G = 1000$ W/m^2 (7.55 A for Gruposolar GS601456P-218 and 6.87 A for Sanyo HIP-230 HDE1), these differences correspond to a percentage error of 5.2% and 21.3%, respectively. At a constant irradiance of $G = 1000$ W/m^2 and $T \neq 25$ °C the maximum differences for current calculated by the models are 0.605 A and 1.456 A, respectively. Compared to the measured values of current at the maximum power point with $G = 1000$ W/m^2 these differences correspond to a percentage error of 8.01% and 21.2%, respectively.

Tables 7 and 8 list the absolute mean differences of current and of power between the measured and the calculated data.

At a constant temperature of $T = 25$ °C, the absolute mean differences for current calculated by the new model and the Saloux et al. model are 0.100 A and 0.341 A, respectively. If compared to the measured values of current at the maximum power point with $G = 1000$ W/m^2 these differences correspond to a percentage error of 1.32% and 4.96%, respectively. The absolute mean differences for power calculated by the new model and the Saloux et al. model are 3.118 W and 13.342 W, respectively. Compared to the measured values of the maximum power point with $G = 1000$ W/m^2 (218.95 W for Gruposolar GS601456P-218 and 233.58 W for Sanyo HIP-230 HDE1) these differences correspond to a percentage error of 1.42% and 5.71%, respectively.

At a constant irradiance of $G = 1000$ W/m^2 and $T \neq 25$ °C the absolute mean differences for current calculated by the models are 0.160 A and 0.281 A, respectively. If compared to the measured values of current at the maximum power point with $G = 1000$ W/m^2 these differences correspond to a percentage error of 2.12% and 4.09%, respectively. The absolute mean differences for power calculated by the new model and the Saloux et al. model are 4.317 W and 9.993 W, respectively. Compared to the measured values of the maximum power point with $G = 1000$ W/m^2 these differences correspond to a percentage error of 1.97% and 4.28%, respectively.

The accuracy of the new model, which is almost always more precise than the Saloux et al. model, is quite satisfactory. Even in worst case, the new model calculates the *I–V* characteristics with an error smaller than the data tolerance usually declared by the manufacturer, which usually is +10/−5% for maximum power at SRC.

5. Conclusions

The procedure to evaluate the parameters of a new one-diode PV panel model by means of the performance data provided in a tabular form is described. The five parameters R_s, R_{sh}, n, I_L and I_0 are obtained by imposing on both the calculated *I–V* characteristics and those measured by manufacturers the following conditions: equality of the short circuit current, equality of the open circuit voltage, correspondence of the maximum power point and equal values of the curve derivative in the points of short circuit and open circuit for nominal conditions. The thermal performance of the proposed model is improved by means of a coefficient that is calculated using the maximum power temperature coefficient, which is a data usually provided by manufacturers. The computer routines used to evaluate the values of the above parameters are listed; the routines are written in BASIC and can be easily implemented, even like VBA macros in Microsoft Excel.

To skirt the obstacle of the determination of resistances R_{so} and R_{sho} and open voltage V_{oc} at various irradiances, which only can be extracted from the graphical data provided by manufacturers, three analytical correlations were defined on the basis of the performance data of more than one hundred surveyed PV panels.

The capability of the new model to calculate the I–V characteristics was tested by comparing the results with the data measured by four different manufacturers. Furthermore a comparison with the Saloux et al. model, which is a simplified one-diode model that can does not requires the information derived from the graphical data, was made. The new model in most cases resulted more precise than the Saloux et al. model. At a constant temperature of $T = 25$ °C, the absolute mean differences between current and power values calculated by the new model and the measured values are 1.19% and 1.42% of the nominal current and power at maximum power point respectively. At a constant irradiance of $G = 1000$ W/m^2 and $T \neq 25$ °C, the above absolute mean differences are 2.12% and 1.97 of the nominal current and power at maximum power point respectively.

The results of the application of the new model confirm the reliability of the proposed procedure. The differences between the calculated and the measured data are always less than the data tolerance usually declared by the manufacturers. Thanks to the new model, even for the PV panels whose technical data are only provided in a tabular form, it is possible to get very accurate energy performance predictions.

Appendix A

Tables A1 and A2.

Table A1
Values of resistances R_{so} and R_{sho} (Part 1).

No.	Manufacturer	Model	Type	I_s (A)	V_{oc} (V)	V_{oc}/I_{sc} (Ω)	R_{so} (Ω)		R_{sho} (Ω)	
							Meas.	Calc.	Meas.	Calc.
1	Alfa Solar	Pyramid 54-210	P	8.89	33.49	3.77	0.53	0.42	133	130
2	Alfa Solar	Pyramid 60-237	P	9.00	37.37	4.15	0.69	0.46	184	143
3	Alfa Solar	Pyramid 80-311	P	8.95	49.37	5.52	0.42	0.62	190	190
4	Alpex Solar	ALP 240	P	8.49	37.38	4.40	0.65	0.49	183	152
5	Amerisolar	AS-5M 170	M	5.25	43.60	8.30	0.89	0.93	220	287
6	Amerisolar	AS-6M27 200	M	8.19	33.00	4.03	0.48	0.45	142	139
7	Amerisolar	AS-6M30 230	M	8.31	36.90	4.44	0.44	0.50	129	153
8	Amerisolar	AS-6P27 200	P	8.24	32.80	3.98	0.38	0.45	107	137
9	Amerisolar	AS-6M24 190	M	8.20	29.80	3.63	0.35	0.41	117	125
10	Amerisolar	AS-6P24 195	M	8.30	30.00	3.61	0.29	0.40	142	125
11	Amerisolar	AS-6P205	P	7.49	36.30	4.85	0.54	0.54	144	167
12	Amerisolar	AS-6P215	P	7.79	36.40	4.67	0.40	0.52	139	161
13	Amerisolar	AS-6P220	P	7.94	36.50	4.60	0.51	0.51	135	159
14	AstroPower	AP-65	M	4.70	20.50	4.36	0.81	0.49	106	151
15	AstroPower	AP-100	M	7.20	20.10	2.79	0.38	0.31	97	96
16	AstroPower	AP-1106	M	7.50	20.70	2.76	0.44	0.31	85	95
17	AstroPower	AP-1206	M	7.70	21.00	2.73	0.51	0.30	86	94
18	Azur Solar	M 180U-3	M	8.62	29.40	3.41	0.47	0.38	83	118
19	Azur Solar	M 245-3	M	5.35	61.10	11.42	0.93	1.28	519	394
20	Bisol	BMU/227	P	8.35	37.10	4.44	0.64	0.50	171	153
21	Canadian Solar	CS5A-190M	M	5.52	44.80	8.12	0.71	0.91	395	280
22	Canadian Solar	CS5A-175P	P	5.31	44.10	8.31	0.73	0.93	398	287
23	Canadian Solar	CS5A-250M	M	5.49	59.60	10.86	0.95	1.21	369	375
24	Canadian Solar	CS5A-235P	P	5.31	58.80	11.07	0.98	1.24	497	382
25	Canadian Solar	CS6A-185M	M	8.26	29.70	3.60	0.45	0.40	196	124
26	Canadian Solar	CS6A-180P	P	8.19	29.40	3.59	0.54	0.40	198	124
27	Canadian Solar	CS6P-235M	M	8.34	37.20	4.46	0.51	0.50	295	154
28	Canadian Solar	CS6P-230P	P	8.34	36.80	4.41	0.57	0.49	198	152
29	CentroSolar	D230	P	8.34	36.80	4.41	0.42	0.49	161	152
30	Day4 Energy	48MC 175	P	8.05	29.20	3.63	0.48	0.41	218	125
31	Day4 Energy	60MC-I 235	P	8.42	36.90	4.38	0.51	0.49	223	151
32	DelSolar	D6M245B3A	M	8.64	37.48	4.34	0.53	0.48	125	150
33	DelSolar	D6P240B3A	P	8.38	37.83	4.51	0.60	0.50	108	156
34	DelSolar	D6M140B1A	M	8.54	22.11	2.59	0.31	0.29	98	89
35	DelSolar	D6M195B2A	M	8.64	29.87	3.46	0.45	0.39	97	119
36	DelSolar	D6P140B1A	P	8.34	22.26	2.67	0.36	0.30	85	92
37	DelSolar	D6P180A2E	P	8.27	29.66	3.59	0.40	0.40	115	124
38	DelSolar	D6P190A35	P	7.93	32.94	4.15	0.35	0.46	149	143
39	FVG Energy	FGV60-156-235M	M	8.28	37.25	4.50	0.36	0.50	108	155
40	FVG Energy	FGV60-156-240P-MC	P	8.28	37.60	4.54	0.48	0.51	107	157
41	GE Energy	GEPVp-066-G	P	8.20	10.90	1.33	0.27	0.15	33	46
42	GE Energy	GEPVp-200-M	P	8.10	32.90	4.06	0.56	0.45	128	140
43	GE Energy	GEPVp-205-M	P	8.20	33.00	4.02	0.55	0.45	126	139
44	Gruposolar	GS601456M-227	M	8.70	36.81	4.23	0.58	0.47	103	146
45	Helios Technology	H3A220P	P	8.06	36.93	4.58	0.53	0.51	140	158
46	Helios Technology	HM3A220P	P	8.16	36.92	4.52	0.53	0.51	138	156

Table A1 (*continued*)

No.	Manufacturer	Model	Type	I_s (A)	V_{oc} (V)	V_{oc}/I_{sc} (Ω)	R_{so} (Ω)		R_{sho} (Ω)	
							Meas.	Calc.	Meas.	Calc.
47	Helios Technology	HMA220	M	8.11	36.95	4.56	0.53	0.51	139	157
48	Isofoton	IS-170	M	5.13	44.60	8.69	0.96	0.97	281	300
49	Isofoton	ISF-200	M	8.17	33.20	4.06	0.50	0.45	129	140
50	Isofoton	ISF-220	M	8.17	36.90	3.77	0.65	0.50	162	156
51	Kyocera	KD135SX-UPU	P	8.37	22.10	4.15	0.37	0.30	80	91
52	Kyocera	KD185GX-LPU	P	8.58	29.50	5.52	0.37	0.38	80	119
53	Kyocera	KD205GX-LPU	P	8.36	33.20	4.40	0.41	0.44	108	137
54	Kyocera	KD210GX-LPU	P	8.58	33.20	8.30	0.41	0.43	105	134
55	Kyocera	KD215GX-LPU	P	8.78	33.20	4.03	0.48	0.42	103	131
56	Kyocera	KD235GX-LPB	P	8.55	36.90	4.44	0.58	0.48	159	149
57	Kyocera	KD130GX-LP	P	8.06	22.10	3.98	0.35	0.31	62	95
58	Kyocera	KD135GX-LP	P	8.37	22.10	3.63	0.28	0.30	75	91
59	Kyocera	KD180GX-LP	P	8.35	29.50	3.61	0.46	0.39	125	122
60	Kyocera	KD205GX-LP	P	8.36	33.20	4.85	0.38	0.44	124	137
61	Kyocera	KD210GX-LP	P	8.58	33.20	4.67	0.44	0.43	125	134
62	Kyocera	KC40T	P	2.65	21.70	4.60	0.89	0.92	175	283
63	Kyocera	KC50T	P	3.31	21.70	4.36	0.97	0.73	184	226
64	Kyocera	KC65T	P	3.99	21.70	2.79	0.68	0.61	139	188
65	Kyocera	KC85T	P	5.34	21.70	2.76	0.44	0.45	87	140
66	Kyocera	KC130GT	P	8.02	21.90	2.73	0.35	0.31	84	94
67	Kyocera	KC175GT	P	8.09	29.20	3.41	0.54	0.40	84	125
68	Kyocera	KC200GT	P	8.21	32.90	11.42	0.46	0.45	124	138
69	Ligitek Photovoltaic	LM090AA00	M	5.35	22.35	4.44	0.34	0.47	186	144
70	Ligitek Photovoltaic	LM090AB00	P	5.33	22.35	8.12	0.34	0.47	183	145
71	Ligitek Photovoltaic	LM140BA00	M	8.49	22.36	8.31	0.27	0.29	68	91
72	Ligitek Photovoltaic	LM140BB00	P	8.27	22.25	10.86	0.36	0.30	104	93
73	Ligitek Photovoltaic	LM195BA02	M	8.77	30.10	11.07	0.52	0.38	129	118
74	Ligitek Photovoltaic	LM210BB04	P	8.45	33.54	3.60	0.58	0.44	103	137
75	Ligitek Photovoltaic	LM215BA04	M	8.63	33.75	3.59	0.57	0.44	101	135
76	Lorentz	LA30-12S	M	1.90	21.00	4.46	1.00	1.24	361	381
77	Lorentz	LA55-12S	M	3.70	20.10	4.41	0.52	0.61	181	187
78	Lorentz	LA80-12S	M	5.30	20.20	4.41	0.36	0.43	137	132
79	Lorentz	LA95-12S	M	6.20	20.60	3.63	0.37	0.37	117	115
80	Lorentz	LA100-12S	M	6.30	21.20	4.38	0.24	0.38	116	116
81	Lorentz	LA130-12S	M	7.10	24.10	4.34	0.32	0.38	103	117
82	Lorentz	LA170-24S	M	5.80	39.20	4.51	0.59	0.76	252	233
83	Lorentz	LC40-12M	M	2.60	21.70	2.59	0.74	0.93	275	288
84	Lorentz	LC50-12M	M	3.20	21.60	3.46	0.71	0.75	206	233
85	Lorentz	LC75-12M	M	4.80	21.60	2.67	0.40	0.50	138	155
86	Lorentz	LC80-12M	M	5.00	21.60	3.59	0.46	0.48	149	149
87	Lorentz	LC120-12P	P	7.70	21.40	4.15	0.35	0.31	92	96
88	Lorentz	LC175-24M	M	5.40	44.40	4.50	0.84	0.92	236	284
89	Martifer	MTS215P	P	8.06	36.47	4.54	0.71	0.51	223	156
90	Martifer	MTS220P	P	8.18	36.93	1.33	0.75	0.50	222	156
91	Martifer	MTS225P	P	8.32	37.11	4.06	0.73	0.50	168	154
92	Martifer	MTS230P	P	8.33	37.35	4.02	0.42	0.50	168	155
93	Photowatt	PW6-110-110	P	6.90	21.70	4.23	0.38	0.35	104	109
94	Photowatt	PW6-123-120	P	7.40	21.90	4.51	0.41	0.33	75	102
95	Photowatt	PW500-50	P	3.20	21.60	4.58	0.82	0.75	216	233
96	Renergies Italia	REN170M/170	M	5.07	44.35	4.52	1.06	0.98	216	302
97	Sanyo	195BKB5	HIP	3.79	78.10	20.61	3.19	3.32	2,232	2,565
98	Sanyo	210NKHB5	HIP	5.57	50.90	9.14	1.34	1.47	1,336	1,138
99	Sanyo	215NKHE5	HIP	5.61	51.60	9.20	1.53	1.48	1,163	1,145
100	Sanyo	240HDE4	HIP	7.37	43.60	5.92	0.92	0.95	912	736
101	Sanyo	N220E01	HIP	5.72	50.90	8.90	1.39	1.44	1,046	1,108
102	Sanyo	180BA19	HIP	3.65	66.40	18.19	3.07	2.93	2,329	2,265
103	Sanyo	190BA19	HIP	3.75	67.50	18.00	2.84	2.90	2,341	2,241
104	Sanyo	186BA20	HIP	3.71	67.00	18.06	3.66	2.91	2,357	2,248
105	Sanyo	195BA19	HIP	3.79	68.10	17.97	2.93	2.90	2,380	2,237
106	Sanyo	200BA19	HIP	3.83	68.70	17.94	2.56	2.89	2,104	2,233
107	Sanyo	205BA20	HIP	3.84	68.80	17.92	2.54	2.89	2,115	2,230
108	Sanyo	205NKHA5	HIP	5.54	50.30	9.08	1.50	1.46	1,199	1,130
109	Sanyo	210NKHA5	HIP	5.57	50.90	9.14	1.52	1.47	1,177	1,138
110	Sanyo	215NKHA5	HIP	5.61	51.60	9.20	1.51	1.48	1,174	1,145
111	Shell	S25	P	1.50	21.40	4.56	1.08	1.59	540	492
112	Shell	S36	P	2.30	21.40	8.69	1.15	1.04	330	321
113	Shell	SM50-H	P	3.35	19.80	4.06	0.48	0.66	272	204
114	Shell	S65	P	4.30	20.90	4.86	0.88	0.54	109	168
115	Shell	S105	P	4.50	31.80	7.07	0.83	0.79	327	244
116	Shell	SM110-12P	M	6.90	21.70	3.14	0.31	0.35	207	109
117	Shell	S115	P	4.70	32.80	6.98	0.80	0.78	328	241
118	Solarday	PX60-220	P	8.29	37.10	4.48	0.74	0.50	182	154
119	Solarfun	SF 190-27-M-195	M	8.12	32.90	4.05	0.39	0.45	91	140

(*continued on next page*)

Table A1 (*continued*)

No.	Manufacturer	Model	Type	I_s (A)	V_{oc} (V)	V_{oc}/I_{sc} (Ω)	R_{so} (Ω)		R_{sho} (Ω)	
							Meas.	Calc.	Meas.	Calc.
120	Solarfun	SF 190-27-M-195	P	8.06	32.70	4.06	0.39	0.45	106	140
121	Solarfun	SF 160-24-P-170	P	5.17	44.10	8.53	0.85	0.95	224	294
122	Solaria	S6P235	P	8.66	37.76	4.36	0.57	0.49	107	150
123	Suntech	STP170S-24/Ab-1	M	5.14	43.80	8.52	0.65	0.95	259	294
124	Suntech	STP185S-24/Ad	M	5.43	45.00	8.29	0.85	0.93	250	286
125	Suntech	STP195S-24/Ad+	M	5.69	45.40	7.98	0.83	0.89	333	275
126	Suntech	STP210-18/Ud	P	8.33	33.60	4.03	0.36	0.45	169	139
127	Suntech	STP260-24/Vb-1	P	8.09	44.00	5.44	0.40	0.61	227	188
128	Suntech	STP030D-12/LEA	P	1.94	21.60	11.13	1.33	1.24	421	384
129	Suntech	STP040D-12/REA	P	2.58	21.80	8.45	0.95	0.94	346	292
130	Suntech	STP050D-12/MEA	P	3.13	21.80	6.96	0.78	0.78	305	240
131	Suntech	STP060D-12/SEA	P	3.90	21.60	5.54	0.73	0.62	254	191
132	Suntech	STP080B-12/BEA	M	4.95	21.90	4.42	0.60	0.49	176	153
133	Suntech	STP130B-12/TEA	P	8.09	22.00	2.72	0.27	0.30	131	94
134	Topsola	TSM72-125M-G-175	M	5.40	44.00	8.15	1.33	0.91	173	281
135	Topsola	TSM96-125M-220	M	5.25	57.85	11.02	1.35	1.23	245	380
136	Topsola	TSM-160M-180	M	5.45	44.50	8.17	1.18	0.91	237	282
137	Topsola	TSM-40M-45	M	2.71	22.10	8.15	1.38	0.91	158	281
138	Topsola	TSM-50M-55	M	3.32	22.10	6.66	1.12	0.74	128	230
139	Topsola	TSM-75M-85	M	5.28	22.35	4.23	0.64	0.47	93	146
140	Trinasolar	TSM-180DC01	M	5.35	44.20	8.26	0.85	0.92	283	285
141	Trinasolar	TSM-230PC05	P	8.26	37.00	4.48	0.51	0.50	149	155
142	Yocasol	LDA170	M	5.44	44.30	8.14	1.19	0.91	357	281
143	Yocasol	PCA200	M	8.68	32.80	3.78	0.48	0.42	165	130
144	Yocasol	PCB190	P	8.18	32.30	3.95	0.46	0.44	165	136

Table A2
Values of the open circuit voltage at various irradiances (Part 1).

No.	Manufacturer	Model	Type	Open circuit voltage V_{oc} (V) Irradiance G (kW/m^2)					Scaled open circuit voltage $V_{oc}/V_{oc,ref}$ Irradiance G (kW/m^2)				
				1.00	0.80	0.60	0.40	0.20	1.00	0.80	0.60	0.40	0.20
1	Aide Solar	XZST-190(M)	M	33.2	33.0	32.5	–	–	1.00	0.994	0.979	–	–
2	Aide Solar	XZST-190	P	33.2	32.9	32.5	–	–	1.00	0.991	0.979	–	–
3	Ait-Tech	AIT-6 225-60	P	36.8	36.3	35.6	34.8	–	1.00	0.986	0.967	0.946	–
4	Alex Solar	ALM 175D-24	M	44.2	43.6	42.8	–	–	1.00	0.986	0.968	–	–
5	Alfa Solar	Pyramid 60-237	P	37.4	37.0	36.4	35.6	34.3	1.00	0.990	0.974	0.953	0.918
6	Alfa Solar	Pyramid 54-210	P	33.5	33.0	32.5	31.9	30.8	1.00	0.985	0.970	0.953	0.920
7	Alfa Solar	Pyramid 80-311	P	49.4	48.9	48.3	47.1	45.8	1.00	0.990	0.978	0.954	0.928
8	Alpex Solar	ALP 240	P	37.4	36.8	36.2	35.2	33.9	1.00	0.984	0.968	0.942	0.907
9	Amerisolar	AS-5M 170	M	43.6	43.3	–	42.2	41.0	1.00	0.993	–	0.968	0.940
10	Amerisolar	AS-6M24 190	M	29.8	29.4	28.7	28.2	27.4	1.00	0.987	0.963	0.946	0.919
11	Amerisolar	AS-6P24 195	M	30.0	29.5	28.8	28.3	27.6	1.00	0.983	0.960	0.943	0.920
12	Azur Solar	M 245-3	M	61.1	60.6	59.9	–	–	1.00	0.992	0.980	–	–
13	Azur Solar	M 180U-3	M	29.4	29.2	29.0	28.5	27.8	1.00	0.993	0.986	0.969	0.946
14	Bisol	BMU/227	P	37.1	36.8	36.4	35.8	34.2	1.00	0.992	0.981	0.965	0.922
15	Canadian Sol.	CS5A-190M	M	44.8	44.4	43.8	43.0	–	1.00	0.991	0.978	0.960	–
16	Canadian Sol.	CS5A-175P	P	44.1	43.7	43.1	42.6	–	1.00	0.991	0.977	0.966	–
17	Canadian Sol.	CS5A-250M	M	59.6	59.1	58.3	57.3	–	1.00	0.992	0.978	0.961	–
18	Canadian Sol.	CS5A-235P	P	58.8	58.3	57.5	56.5	–	1.00	0.991	0.978	0.961	–
19	Canadian Sol.	CS6A-185M	M	29.7	29.4	29.0	28.7	–	1.00	0.990	0.976	0.966	–
20	Canadian Sol.	CS6A-180P	P	29.4	29.1	28.7	28.2	–	1.00	0.990	0.976	0.959	–
21	Canadian Sol.	CS6A-235M	M	37.2	37.0	36.5	36.0	–	1.00	0.995	0.981	0.968	–
22	Canadian Sol.	CS6A-230P	P	36.8	36.6	36.1	35.3	–	1.00	0.995	0.981	0.959	–
23	Day4 Energy	48MC 175	P	29.2	28.9	–	–	26.9	1.00	0.990	–	–	0.921
24	Day4 Energy	60MC-I 235	P	36.9	36.5	–	–	34.2	1.00	0.989	–	–	0.927
25	DelSolar	D6P180A2E	P	29.7	29.0	28.5	–	–	1.00	0.978	0.961	–	–
26	DelSolar	D6P190A35	P	32.9	32.6	32.2	–	–	1.00	0.990	0.978	–	–
27	DelSolar	D6P140B1A	P	22.3	22.0	21.6	21.2	20.4	1.00	0.988	0.970	0.952	0.916
28	DelSolar	D6M245B3A	M	37.5	37.0	36.4	35.7	34.4	1.00	0.987	0.971	0.953	0.918
29	DelSolar	D6M140B1A	M	22.1	21.8	21.5	21.1	20.3	1.00	0.986	0.972	0.954	0.918
30	DelSolar	D6P240B3A	P	37.8	37.4	36.9	36.1	34.8	1.00	0.989	0.975	0.954	0.920
31	DelSolar	D6M195B2A	M	29.9	29.5	29.1	28.4	27.5	1.00	0.988	0.974	0.951	0.921
32	FVG Energy	60-156-235M	M	37.3	36.7	36.0	35.4	34.7	1.00	0.985	0.966	0.950	0.932
33	FVG Energy	60-156-240P-MC	P	37.6	36.9	36.1	35.6	34.7	1.00	0.981	0.960	0.947	0.923
34	Gruposolar	GS601456M-227	M	36.8	36.3	35.6	34.7	33.2	1.00	0.986	0.967	0.943	0.902
35	Helios Tech.	HM3A220P	P	36.9	36.4	35.9	35.5	33.9	1.00	0.986	0.972	0.962	0.918
36	Helios Tech.	HMA220	M	37.0	36.5	36.0	35.4	34.0	1.00	0.988	0.974	0.958	0.920
37	Helios Tech.	H3A220P	P	36.9	36.4	35.9	35.3	34.0	1.00	0.986	0.972	0.956	0.921
38	Kyocera	KC65T	P	21.7	21.3	21.0	20.4	19.6	1.00	0.982	0.968	0.940	0.903
39	Kyocera	KD180GX-LP	P	29.5	29.1	28.6	28.0	26.7	1.00	0.986	0.969	0.949	0.905

Table A2 (*continued*)

No.	Manufacturer	Model	Type	Open circuit voltage V_{oc} (V) Irradiance G (kW/m^2)					Scaled open circuit voltage $V_{oc}/V_{oc.ref}$ Irradiance G (kW/m^2)				
				1.00	0.80	0.60	0.40	0.20	1.00	0.80	0.60	0.40	0.20
40	Kyocera	KD210GX-LPU	P	33.2	32.9	32.6	31.9	31.2	1.00	0.991	0.982	0.961	0.940
41	Kyocera	KD215GX-LPU	P	33.2	32.8	32.5	31.9	31.2	1.00	0.988	0.979	0.961	0.940
42	Kyocera	KD135SX-UPU	P	22.1	21.6	21.2	20.7	20.2	1.00	0.977	0.959	0.937	0.914
43	Kyocera	KD130GX-LP	P	22.1	21.5	21.1	20.7	20.2	1.00	0.973	0.955	0.937	0.914
44	Kyocera	KD135GX-LP	P	22.1	21.6	21.1	20.7	20.2	1.00	0.977	0.955	0.937	0.914
45	Kyocera	KD185GX-LPU	P	29.5	29.2	28.9	28.5	27.7	1.00	0.990	0.980	0.966	0.939
46	Kyocera	KD205GX-LPU	P	33.2	32.9	32.6	32.1	31.1	1.00	0.991	0.982	0.967	0.937
47	Kyocera	KD205GX-LP	P	33.2	32.8	32.4	31.9	31.1	1.00	0.988	0.976	0.961	0.937
48	Kyocera	KC50T	P	21.7	21.4	21.1	20.9	19.9	1.00	0.986	0.972	0.963	0.917
49	Kyocera	KC40T	P	21.7	21.5	21.2	20.8	20.3	1.000	0.991	0.977	0.959	0.935
50	Kyocera	KD210GX-LP	P	33.2	32.8	32.4	31.9	31.0	1.00	0.988	0.976	0.961	0.934
51	Kyocera	KC130GT	P	21.9	21.6	21.4	21.1	20.4	1.00	0.986	0.977	0.963	0.932
52	Kyocera	KC85T	P	21.7	21.5	21.2	20.8	20.0	1.00	0.991	0.977	0.959	0.922
53	Kyocera	KC175GT	P	29.2	28.8	28.2	27.7	27.0	1.00	0.986	0.966	0.949	0.925
54	Kyocera	KC200GT	P	32.9	32.5	32.1	31.5	30.5	1.00	0.988	0.976	0.957	0.927
55	Kyocera	KD235GX-LPB	P	36.9	36.6	36.2	35.5	34.2	1.00	0.992	0.981	0.962	0.927
56	Ligitek Phot.	LM090AA00	M	22.4	22.0	21.5	–	–	1.00	0.984	0.962	–	–
57	Ligitek Phot.	LM090AB00	P	22.4	22.1	21.5	–	–	1.00	0.989	0.962	–	–
58	Ligitek Phot.	LM140BA00	M	22.4	22.0	21.5	–	–	1.00	0.984	0.962	–	–
59	Ligitek Phot.	LM140BB00	P	22.3	21.8	21.3	–	–	1.00	0.980	0.957	–	–
60	Ligitek Phot.	LM185AA00	M	45.1	44.7	44.1	–	–	1.00	0.991	0.978	–	–
61	Ligitek Phot.	LM185AB00	P	45.0	44.7	44.0	–	–	1.00	0.993	0.978	–	–
62	Ligitek Phot.	LM195BA02	M	30.1	29.5	29.3	–	–	1.00	0.980	0.973	–	–
63	Ligitek Phot.	LM210BB04	P	33.5	32.9	32.1	–	–	1.00	0.981	0.957	–	–
64	Ligitek Phot.	LM215BA04	M	33.8	33.0	32.3	–	–	1.00	0.978	0.957	–	–
65	Sanyo	186BA19	HIP	67.0	66.3	65.4	64.1	62.1	1.00	0.990	0.976	0.957	0.927
66	Sanyo	205NKHA5	HIP	50.3	49.9	49.1	48.2	46.8	1.00	0.992	0.976	0.958	0.930
67	Sanyo	215NKHE5	HIP	51.6	51.2	50.4	49.5	48.0	1.00	0.992	0.977	0.959	0.930
68	Sanyo	195BA19	HIP	68.1	67.4	66.4	65.2	63.3	1.00	0.990	0.975	0.957	0.930
69	Sanyo	180BA19	HIP	66.4	65.8	64.9	63.7	61.7	1.00	0.991	0.977	0.959	0.929
70	Sanyo	215NKHA5	HIP	51.6	51.1	50.3	49.4	47.9	1.00	0.990	0.975	0.957	0.928
71	Sanyo	210NKHB5	HIP	50.9	50.3	49.6	48.6	47.1	1.00	0.988	0.974	0.955	0.925
72	Sanyo	190BA19	HIP	67.5	66.8	65.9	64.6	62.6	1.00	0.990	0.976	0.957	0.927
73	Sanyo	N220E01	HIP	50.9	50.4	49.6	48.6	47.2	1.00	0.990	0.974	0.955	0.927
74	Sanyo	210NKHA5	HIP	50.9	50.4	49.6	48.7	47.2	1.00	0.990	0.974	0.957	0.927
75	Sanyo	200BA19	HIP	68.7	68.0	67.0	65.8	63.7	1.00	0.990	0.975	0.958	0.927
76	Sanyo	205BA19	HIP	68.8	68.3	67.1	65.9	63.7	1.00	0.993	0.975	0.958	0.926
77	Sanyo	195BKB5	HIP	78.1	77.3	76.3	74.9	72.4	1.00	0.990	0.977	0.959	0.927
78	Sanyo	186BA20	HIP	67.0	66.3	65.4	64.1	62.1	1.00	0.990	0.976	0.957	0.927
79	Shell	S10	P	21.4	21.1	20.9	20.4	19.6	1.00	0.986	0.977	0.953	0.916
80	Shell	S25	P	21.4	21.2	21.0	20.6	20.0	1.00	0.991	0.981	0.963	0.935
81	Shell	S36	P	21.4	21.2	20.8	20.3	19.5	1.00	0.991	0.972	0.949	0.911
82	Shell	SM50-H	P	19.8	19.6	19.4	19.0	18.4	1.00	0.990	0.980	0.960	0.929
83	Shell	S65	P	20.9	20.7	20.4	20.0	19.2	1.00	0.990	0.976	0.957	0.919
84	Shell	SP75	M	21.7	21.4	21.2	20.7	20.0	1.00	0.986	0.977	0.954	0.922
85	Shell	S105	P	31.8	31.4	31.0	30.2	29.3	1.00	0.987	0.975	0.950	0.921
86	Shell	SM110-12P	M	21.7	21.5	21.2	20.5	19.8	1.00	0.991	0.977	0.945	0.912
87	Shell	S115	P	32.8	32.4	32.1	31.4	30.0	1.00	0.988	0.979	0.957	0.915
88	Solarday	PX60-220	P	37.1	36.6	36.0	35.3	34.0	1.00	0.987	0.970	0.951	0.916
89	Solarfun	SF 160-24-P-170	P	44.1	43.7	–	42.6	41.5	1.00	0.991	–	0.966	0.941
90	Suntech	STP170S-24/Ab-1	M	43.8	43.4	42.8	–	–	1.00	0.991	0.977	–	–
91	Suntech	STP200-18/Ub1	P	33.4	33.0	32.8	–	–	1.00	0.988	0.982	–	–
92	Suntech	STP260-24/Vb-1	P	44.0	43.5	42.9	–	–	1.00	0.989	0.975	–	–
93	Suntech	STP030D-12/LEA	P	21.6	21.3	20.9	–	–	1.00	0.986	0.968	–	–
94	Suntech	STP040D-12/REA	P	21.8	21.5	21.2	–	–	1.00	0.986	0.972	–	–
95	Suntech	STP050D-12/MEA	P	21.8	21.5	21.2	–	–	1.00	0.986	0.972	–	–
96	Suntech	STP060D-12/SEA	P	21.6	21.3	21.0	–	–	1.00	0.986	0.972	–	–
97	Suntech	STP080B-12/BEA	M	21.9	21.6	21.3	–	–	1.00	0.986	0.973	–	–
98	Suntech	STP130B-12/TEA	P	22.0	21.6	21.3	–	–	1.00	0.982	0.968	–	–
99	Suntech	STP210-18/Ud	P	33.6	33.3	32.7	32.0	30.8	1.00	0.991	0.973	0.952	0.917
100	Suntech	STP185S-24/Ad	M	45.0	44.6	44.2	43.2	42.1	1.00	0.991	0.982	0.960	0.936
101	Suntech	STP210-18/Ud	P	33.6	33.3	32.7	32.0	30.8	1.00	0.991	0.973	0.952	0.917
102	Suntech	STP185S-24/Ad	M	45.0	44.6	44.2	43.2	42.1	1.00	0.991	0.982	0.960	0.936
101	Suntech	STP210-18/Ud	P	33.6	33.3	32.7	32.0	30.8	1.00	0.991	0.973	0.952	0.917
102	Suntech	STP185S-24/Ad	M	45.0	44.6	44.2	43.2	42.1	1.00	0.991	0.982	0.960	0.936
101	Suntech	STP195S-24/Ad+	M	45.4	45.1	44.6	43.5	41.7	1.00	0.993	0.982	0.958	0.919
102	Topsola	TSM96-125M-220	M	57.9	57.1	56.3	55.4	54.6	1.00	0.987	0.973	0.958	0.944
103	Topsola	TSM-75M-85	M	22.4	22.0	21.5	21.1	20.5	1.00	0.984	0.962	0.944	0.917
104	Topsola	TSM-50M-55	M	22.1	21.7	21.3	20.9	20.3	1.00	0.982	0.964	0.946	0.919
105	Topsola	TSM72-125M-G-175	M	44.0	43.3	42.7	41.9	40.9	1.00	0.984	0.970	0.952	0.930
106	Topsola	TSM-40M-45	M	22.1	21.7	21.3	21.0	20.5	1.00	0.982	0.964	0.950	0.928
107	Topsola	TSM-160M-180	M	44.5	43.9	43.1	42.4	41.2	1.00	0.987	0.969	0.953	0.926
108	Trinasolar	TSM-230DC05	P	37.0	36.4	35.6	35.0	34.1	1.00	0.984	0.962	0.946	0.922

Appendix B

BASIC computer routine for the evaluation of I_0, n and R_s at STC.

BASIC computer routine for the evaluation of I_0, n and R_s at STC.

```
'DATA INPUT (G = 1000 W/m² ; T = 25°C)
Voc              'Open Circuit Voltage from Eq.(26)
Isc              'Short Circuit Current
Vmp              'Maximum Power Voltage
Imp              'Maximum Power Current
Rsho             'Inverse of slope at the Short Circuit point from Eqs.(21)
Rso              'Inverse of slope at the Open Circuit point from Eqs.(21)
T = 25 + 273.15  'Temperature in Kelvin degrees

'DATA SCALING
Vrange = Voc
Irange = Isc
Voc = Voc / Vrange
Isc = Isc / Irange
Vmp = Vmp / Vrange
Imp = Imp / Irange
Rsho = Rsho / Vrange * Irange
Rso = Rso / Vrange * Irange

'Rs Trial & Error Process
Accuracy = 0.00001
Rs = 0.01               'Rs -> Series Resistance
Step = 0.001
Sign1 = 1
Start:
'Equation (20) (V=Vmp I=Imp) ; n -> Diode quality factor
nT = (Vmp + Imp * Rs - Voc) / Log(((Isc - Imp) * Rsho - (Vmp + Imp * Rs)) /
     (Isc * Rsho - Voc))
'Equation (19) (V=Voc I=0) ; Io -> Diode inverse saturation current
Io = (Isc - Voc / Rsho) / (Exp(Voc / nT) - 1)
'Equation (17) (derivative at V=Voc I=0)
Difference = (Io / nT * Exp(Voc / nT) + 1 / Rsho) / (1 + Rs * (Io / nT *
             Exp(Voc / nT) + 1 / Rsho))- 1 / Rso

If Abs(Difference) <= Accuracy Then GoTo Out
Sign2 = Sgn(Difference)
If Sign1 <> Sign2 Then Step = -Step / 3
Rs = Rs + Step
Sign1 = Sign2
GoTo Start
Out:

'RESULT INVERSE SCALING
Rs = Rs * Vrange / Irange
Io = Io * Irange
nT = nT * Vrange
n = nT / T

Print Rs, Io, n
END
```

BASIC computer routine for the evaluation of factor K.

BASIC computer routine for the evaluation of factor K.

```
'DATA INPUT (G = 1000 W/m² ; T = 25°C)
n           'Diode quality factor
IL          'Photocurrent at STC: IL = Isc
Voc         'Open Circuit Voltage at STC
Rsh         'Parallel resistance: Rsh = Rsho
Rs          'Series resistance
Pmp         'Maximum Power at STC
IscCoeff    'Short Circuit Current Thermal Coefficient
VocCoeff    'Open Circuit Voltage Thermal Coefficient
PmaxCoeff   'Maximum Power Thermal Coefficient
Tstar       'Temperature ≠ Tref

Tref = 25 + 273.15
Tstar = Tstar + 273.15
nTstar = n * Tstar
Vocstar = Voc + VocCoeff * (TStar - Tref)
ILstar = IL + IscCoeff * (TStar - Tref)
Iostar = (ILstar - Vocstar / Rsh) / (Exp(Voc / nTstar) - 1)
```

```
'Equation (33):
VdMax = -nTstar * Log(Io / nTstar)
For Count = 1 To 6
'Equation (34):
  Imaxstar = ILstar - Iostar * (Exp(VdMax / nTstar) - 1) - VdMax / Rsh
'Equation (32):
  VdMax = nTstar * (Log((Rsh * (ILstar + Iostar) - 2 * (VdMax - Imax * Rs)) /
          (Rsh * (VdMax - 2 * Imax * Rs))) - Log(Iostar * (1 / nTstar + 1 /
          (VdMax - 2 * Imax * Rs))))
Next Count
Imaxstar = ILstar - Iostar * (Exp(VdMax / nTstar) - 1) - VdMax / Rsh
'Equation (35):
Vmaxstar = VdMax - k * Imax * (T - Tref) - Imax * Rs
'Equation (36):
Pmax = Vmaxstar * Imaxstar
'Equation (37):
Difference = Pmax - Pmp * (1 + PmaxCoeff / 100 * (Tstar - Tref))

If Abs(Difference) <= Accuracy Then GoTo Out
Sign2 = Sgn(Difference)
If Sign1 <> Sign2 Then Step = -Step / 3
k = k + Step
Sign1 = Sign2
GoTo Start
Out:

Print k
END
```

References

[1] Akbaba M, Alattawi MAA. A new model for *I–V* characteristic of solar cell generators and its applications. Solar Energy Mater Solar Cells 1995;37:123–32.
[2] Ortiz-Conde O, Garcia Sanchez FJ, Muci J. New method to extract the model parameters of solar cells from the explicit analytic solutions of their illuminated *I–V* characteristics. Solar Energy Mater Solar Cells 2006;90:352–61.
[3] Shockley W. Electrons and holes in semiconductors. New York: Van Nostrand; 1950.
[4] Millman J, Halkias CC. Electronic devices and circuits. New York: McGrow-Hill; 1967.
[5] Wolf M, Rauscenbach H. Series resistance effects on solar cell measurements. Adv Energy Convers 1963;3:455–79.
[6] Enebish N, Agchbayar D, Dorjkhand S, Baatar D, Ylemj I. Numerical analysis of solar cell current-voltage characteristics. Solar Energy Mater Solar Cells 1993;29:201–8.
[7] Hovinen A. Fitting of the solar cell IV-curve to the two diode model. Phys Scripta 1994;T54:175–6.
[8] Garrido-Alzar CL. Algorithm for extraction of solar cell parameters from *I–V* curve using double exponential model. Renew Energy 1997;10:125–8.
[9] Ishaque K, Salam Z, Taheri H. Simple, fast and accurate two-diode model for photovoltaic modules. Solar Energy Mater Solar Cells 2011;95:586–94.
[10] Sandrolini L, Artioli M, Reggiani U. Numerical method for the extraction of photovoltaic module double-diode model parameters through cluster analysis. Appl Energy 2010;87:442–51.
[11] Ishaque K, Salam Z, Taheri H, Shamsudin A. A critical evaluation of EA computational methods for photovoltaic cell parameter extraction based on two-diode. Solar Energy 2011;85:1768–79.
[12] de Blas MA, Torres JL, Prieto E, Garcia A. Selecting a suitable model for characterizing photovoltaic devices. Renew Energy 2002;25:371–80.
[13] Hadj Arab A, Chenlo F, Benghanem M. Loss-of-load probability of photovoltaic water pumping systems. Solar Energy 2004;76:713–23.
[14] De Soto W, Klein SA, Beckman WA. Improvement and validation of a model for photovoltaic array performance. Solar Energy 2006;80:78–88.
[15] Celik AN, Acikgoz N. Modelling and experimental verification of the operating current of mono-crystalline photovoltaic modules using four-and five-parameter models. Appl Energy 2007;84:1–15.
[16] Lo Brano V, Orioli A, Ciulla G, Di Gangi A. An improved five-parameter model for photovoltaic modules. Solar Energy Mater Solar Cells 2010;94:1358–70.
[17] Saloux E, Teyssedou A, Sorin M. Explicit model of photovoltaic panels ro determine voltages and currents at the maximum power point. Solar Energy 2011;85:713–22.
[18] Ishaque K, Salam Z. An improved modelling method to determine the model parameters of photovoltaic (PV) modules using differential evolution (DE). Solar Energy 2011;85:2349–59.
[19] Skoplaki E, Palyvos JA. On the temperature dependence of photovoltaic module electrical performance: a review of efficiency/power correlations. Solar Energy 2009;83:614–24.
[20] Evans DL. Simplified method for predicting photovoltaic array output. Solar Energy 1981;27:555–60.
[21] Notton G, Cristofari C, Mattei M, Poggi P. Modelling of a double-glass photovoltaic module using finite differences. Appl Therm Eng 2005;25:2854–77.
[22] Kou Q, Klein SA, Beckmann WA. A method for estimating the long-term performance of direct-coupled PV pumping systems. Solar Energy 1998;64:33–40.
[23] Duffie JA, Beckman WA. Solar energy thermal processes. New York: Wiley; 1991.
[24] Zhu Z, Yang H, Jiang R, Wu Q. Investigation of conjugate heat transfer in a photovoltaic wall. Heat Trans – Asian Res 2004;33:117–28.
[25] Beyer HG, Bethke J, Drews A, Heinemann D, Lorenz E, Heilscher G et al. Identification of a general model for the MPP performance of PV-modules for the application in a procedure for the performance check of grid connected systems. In: 19th EC photovoltaic solar energy conference, June 7–11, 2004, Paris, France.
[26] Chow TT, He W, Ji J. Hybrid photovoltaic–thermosyphon water heating system for residential application. Solar Energy 2006;80:298–306.
[27] CLEFS CEA. Influence of temperature on photovoltaic module efficiency. CLEFS CEA – No 50/51 – Winter 2004–2005. p. 119.
[28] PVsyst, Software for photovoltaic systems. University of Geneva ISE – Group energy. FOREL Battelle, bât. D7, route de Drize CH-1227 Carouge Switzerland.
[29] Chenlo F, Fabero F, Alonso MC. A comparative study between indoor and outdoor measurements. Final report of project: testing, norms, reliability and harmonisation. Joule II – Contract No. JOU2-CT92-0178; 1995.